Iron and zinc stable isotope evidence for open-system high-pressure dehydration of antigorite serpentinite in subduction zones

Baptiste Debret, Carlos J Garrido, Marie-Laure Pons, Pierre Bouilhol, Edward Inglis, Vicente López Sánchez-Vizcaíno, Helen Williams

Journal Pre-proofs

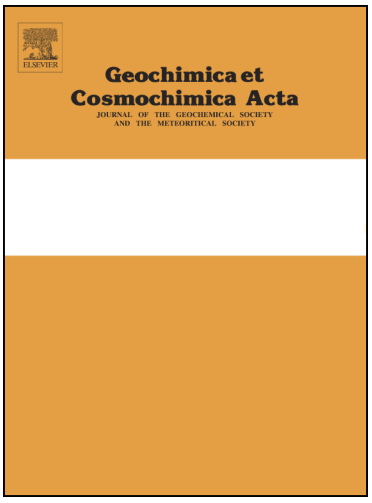

Iron and zinc stable isotope evidence for open-system high-pressure dehydration of antigorite serpentinite in subduction zonesa

Baptiste Debret, Carlos J. Garrido, Marie-Laure Pons, Pierre Bouilhol, Edward Inglis, Vicente López Sánchez-Vizcaíno, Helen Williams

PII: S0016-7037(20)30702-X
DOI: https://doi.org/10.1016/j.gca.2020.12.001
Reference: GCA 12002

To appear in: *Geochimica et Cosmochimica Acta*

Received Date: 11 May 2020
Revised Date: 1 December 2020
Accepted Date: 2 December 2020

Please cite this article as: Debret, B., Garrido, C.J., Pons, M-L., Bouilhol, P., Inglis, E., López Sánchez-Vizcaíno, V., Williams, H., Iron and zinc stable isotope evidence for open-system high-pressure dehydration of antigorite serpentinite in subduction zonesa, *Geochimica et Cosmochimica Acta* (2020), doi: https://doi.org/10.1016/j.gca.2020.12.001

Iron and zinc stable isotope evidence for open-system high-pressure dehydration of antigorite serpentinite in subduction zonesa

Baptiste Debret[1*], Carlos J. Garrido[2], Marie-Laure Pons[3], Pierre Bouilhol[4], Edward Inglis[1], Vicente López Sánchez-Vizcaíno[5], Helen Williams[6]

[1] *Université de Paris, Institut de physique du globe de Paris, CNRS, Paris, France.*
[2] *Instituto Andaluz de Ciencias de la Tierra (IACT), CSIC-UGR, Armilla, Granada, Spain.*
[3] *CEREGE, CNRS, Aix Marseille , IRD, INRAE, Coll France, Aix en Provence, France.*
[4] *Université de lorraine, CRPG/CNRS, 54500 - Nancy, France*
[5] *Departamento de Geología, Escuela Politécnica Superior, Universidad de Jaén (Unidad Asociada al CSIC-IACT Granada), Linares, Jaén, Spain.*
[6] *Department of Earth Sciences, University of Cambridge, Cambridge, UK.*
**corresponding author: ba.debret@gmail.com*

Abstract: Subducted serpentinites have the potential to control the exchange of volatile and redox sensitive elements (e.g., Fe, S, C, N) between the slab, the mantle wedge and the deep mantle. Here we examine the mobility of iron and zinc in serpentinite-derived fluids by using their stable isotopes (δ^{56}Fe and δ^{66}Zn) in high-pressure subducted meta-serpentinites from the Cerro del Almirez massif (Spain). This massif preserves a metamorphic front between antigorite (Atg-serpentinite) and antigorite-olivine-orthopyroxene (transitional lithologies) -bearing serpentinites, and chlorite-bearing harzburgite (Chl-harzburgite), displaying granofels, spinifex and fine-grained recrystallized textures. Those rocks were formed at eclogite facies conditions (1.6–1.9 GPa and 680–710 °C). The mean δ^{56}Fe of all the Cerro del Almirez meta-serpentinites (+0.05 ± 0.01 ‰) is identical within an error to that of primitive mantle (+0.03 ± 0.03 ‰). A positive correlation between δ^{56}Fe and indices of peridotite protolith fertility (e.g., Al_2O_3/SiO_2) suggests that the δ^{56}Fe values of Cerro del Almirez samples predominantly reflect protolith compositional variations, likely produced by prior episodes of melt extraction. In contrast, the Zn concentrations ([Zn] = 34–67 ppm) and isotope signatures (δ^{66}Zn = +0.18 – +0.55 ‰) of the Cerro del Almirez samples show a broad range of values, distinct to those of the primitive mantle ([Zn] = 54 ppm; δ^{66}Zn = +0.16 ± 0.06 ‰). The Atg-serpentinites ([Zn] = 34–46 ppm; δ^{66}Zn = +0.23 ± 0.06 ‰) display similar [Zn] and δ^{66}Zn values to those of slab serpentinites from other high-pressure meta-ophiolites. Both [Zn] and δ^{66}Zn increase in transitional lithologies ([Zn] = 45–67 ppm; δ^{66}Zn = +0.30 ± 0.06 ‰) and Chl-harzburgites with granofels ([Zn] = 38–

59 ppm; $\delta^{66}Zn$ = +0.33 ± 0.04 ‰) or spinifex ([Zn] = 48–66 ppm; $\delta^{66}Zn$ = +0.43 ± 0.09 ‰) textures. Importantly, Cerro del Almirez transitional lithologies and Chl-harzburgites display abnormally high [Zn] relative to abyssal peridotites and serpentinites (29–45 ppm) and a positive correlation exists between [Zn] and $\delta^{66}Zn$. This correlation is interpreted to reflect the mobilization of Zn by subduction zone fluids at high pressures and temperatures coupled with significant Zn stable isotope fractionation. An increase in [Zn] and $\delta^{66}Zn$ from Atg-serpentinite to Chl-harzburgite is associated with an increase in U/Yb, Sr/Y, Ba/Ce and Rb/Ce, suggesting that both [Zn] and $\delta^{66}Zn$ record the interaction of the transitional lithologies and the Chl-harzburgites with fluids that had equilibrated with metasedimentary rocks. Quantitative models show that metasediment derived fluids can have isotopically heavy Zn as a consequence of sediment carbonate dissolution and subsequent Zn complexation with carbonate species in the released fluids (e.g., $[ZnHCO_3(H_2O)^{5+}]$ or $[ZnCO_3(H_2O)_3]$). Our models further demonstrate that Zn complexation with reduced carbon species cannot produce fluids with heavy $\delta^{66}Zn$ signature and hence explain the $\delta^{66}Zn$ variations observed in the Chl-harzburgites. The most straightforward explanation for the heavy $\delta^{66}Zn$ of the Cerro del Almirez samples is thus serpentinite dehydration accompanied by the open system infiltration of the massif by oxidized, carbonate-rich sediment-derived fluids released during prograde subduction-related metamorphism.

1. Introduction

In subduction zones, tracing and quantifying the fluxes of redox-sensitive elements, such as those of iron, carbon or sulfur, between the slab, the mantle wedge and the deep mantle is crucial for understanding Earth chemical evolution and habitability (e.g., Duncan and Dasgupta, 2017). Among subducted lithologies, serpentinites are significant reservoirs of water and redox-sensitive elements (Alt et al., 2013). Their dehydration at depth could, therefore, trigger large scale metasomatism of the mantle wedge area and influence redox sensitive and volatile element cycles between the Earth's interior and surface (Debret and Sverjensky, 2017; Cannao and Malaspina, 2018; Iacovino et al., 2020). However, tracing the cycling of

these elements in subduction zones remains an active research frontier and is subject to considerable uncertainty (e.g., Kelemen and Manning, 2015; Plank and Manning, 2019; Menzel et al., 2020).

One of the main challenges is determining the mobility and speciation of the redox sensitive and volatile elements in fluids released during prograde metamorphism in subduction zones. Although several studies have investigated this problem using traditional stable isotopes (e.g., carbon and sulfur, C and S), the significant overlap between the C and S isotope compositions of seafloor-altered protoliths and high-pressure rocks suggests that these isotope systems are insensitive tracers of geochemical exchanges between the slab and the mantle wedge in subduction zones (e.g., Alt et al., 2013). Non-traditional stable isotopes, such as Fe (δ^{56}Fe) and Zn (δ^{66}Zn), can, however, complement traditional stable isotope systems by providing key constraints on elemental mobility and mass balance as Fe and Zn equilibrium fractionation between different phases (serpentine minerals, Fe-oxides, sulfides, carbonate and fluids) is driven by contrasts in element bonding environment, such as co-ordination chemistry and oxidation state (Polyakov and Mineev, 2000; Schauble, 2004; Fujii et al., 2014). Furthermore, the effects of seafloor alteration (e.g., serpentinization) on Fe and to a lesser extent on Zn isotope systematics of mantle peridotites are comparatively minor (Craddock et al., 2013; Debret et al., 2018a), such that subduction-related fractionation processes should be relatively straightforward to identify. Recent studies have successfully applied Fe and Zn stable isotopes in subduction settings to identify processes associated with high-pressure metamorphism in metabasites, meta-serpentinites and metasedimentary rocks (e.g., Debret et al., 2016; Pons et al., 2016; Inglis et al., 2017; El Korh et al., 2017; Debret et al., 2018b; Turner et al., 2018; Gerrits et al., 2019; Huang et al., 2019; Chen et al., 2019; Debret et al., 2020). In these studies, Fe and Zn stable isotopic variations were attributed to redox reactions and associated metal mobility in sulfur, carbon and chlorine-bearing fluids during metamorphic processes. These results highlight the potential of these isotope systems as powerful tools that can be used to trace redox-sensitive element mobility and quantify redox budget variations associated with prograde metamorphism in subduction zones.

Here we present a study of Fe and Zn isotopes in samples from the eclogite-facies ultramafic massif of Cerro del Almirez (Nevado-Filábride Complex, Betic Cordillera, S. Spain). This massif preserves a unique reaction front between antigorite-bearing serpentinite (Atg-serpentinite) and their high-pressure dehydration product, chlorite-bearing harzburgite (Chl-harzburgite) (Trommsdorff et al., 1998; Padrón-Navarta et al., 2011). Our new data on well-characterized Chl-harzburgite and their precursor Atg-serpentinite allow us to investigate the role of seafloor serpentinization versus subduction dehydration on the distribution and mobility of metals. We show that the change in $\delta^{66}Zn$ observed across the contact between Atg-serpentinites and Chl-harzburgites can be explained by the open-system percolation of external fluids. In this scenario, the $\delta^{66}Zn$ of the Chl-harzburgites are most consistent with metasomatism by carbonate-bearing fluids released during metasedimentary rock devolatilization at high pressures and temperatures.

2. Geological setting

The Cerro del Almirez ultramafic massif lies in the Nevado-Filábride Complex, a subduction complex composed of metapelites, marbles, orthogneisses, meta-serpentinites, and metabasites, exposed in the core of an E–W elongated, antiformal dome structure in the internal zones of the Betics orogenic belt (SE Spain) (Fig. 1a) (Gómez-Pugnaire et al., 2019, and references therein). The Nevado-Filábride Complex results from the subduction of the Mesozoic extended SE Iberian margin beneath the Miocene extended Alborán domain during the westward rollback of the Alpine Tethys slab in the mid-Miocene (15–18 Ma) (López Sánchez-Vizcaíno et al., 2001; Behr and Platt, 2012; Booth-Rea et al., 2015; Gómez-Pugnaire et al., 2019). The complex was then uplifted along the subduction channel and exhumed in the extensional Sierra Nevada antiformal dome (Fig. 1a) (Martínez-Martínez et al., 2002; Behr and Platt, 2012; Booth-Rea et al., 2015).The Cerro del Almirez massif is the largest (2.3 km^2) of several ultramafic massifs that occur along shear zones in the uppermost units of the Nevado-Filábride Complex (Fig. 1b) (Trommsdorff et al., 1998; Martínez-Martínez et al., 2002; Padrón-Navarta et al., 2011). The massif is composed of strongly foliated antigorite-bearing serpentinites (Atg-serpentinites) overlying a 70–100 m sequence of unfoliated, coarse-grained chlorite-bearing harzburgites (Chl-harzburgites). The Atg-serpentinites are made up of antigorite (Atg) +

olivine (Ol) + chlorite (Chl) + magnetite (Mag) + ilmenite (Ilm) ± diopside (Di) ± tremolite (Tr) ± titanian clinohumite (Ti-Chu). The Chl-harzburgites were formed by dehydration of Atg-serpentinites during subduction (Trommsdorff et al., 1998). They are composed of Ol + orthopyroxene (Opx) + Chl + Mag + Ilm ± titano-hematite ± Tr ± Ti-Chu. Two main textures, namely granofels and spinifex, were identified in the Chl-harzburgites (Padrón-Navarta et al., 2011). Granofels Chl-harzburgites are made up of coarse anhedral olivine, chlorite flakes, and prismatic orthopyroxene, with an interlocked texture, whereas spinifex-textured Chl-harzburgites are characterized by a criss-cross arrangement of olivine single crystals (up to 12 cm in length), and by centimetre-scale radial aggregates of orthopyroxene with variable grain size and orientation. Granofels and spinifex Chl-harzburgites occur in interspersed lenses that are thought to record, respectively, sequences of slow and fast fluid draining events during serpentinite dehydration (Padrón-Navarta et al., 2011; Dilissen et al., 2018). Both textural types of Chl-harzburgite are locally recrystallized along grain size reduction zones (Padron-Navarta et al., 2010a). This grain size reduction is also accompanied by a decrease of orthopyroxene modal amount and a change of olivine color, from brown to colorless. These features have been interpreted in terms of reaction pathways for fluid flow during high pressure metamorphism (Padrón-Navarta et al., 2010a). The minimum temperature of crystallization of Chl-harzburgites is constrained by the limit of antigorite stability field, between 660 and 680 °C at 1.6 and 2.5 GPa (e.g., Ulmer and Trommsdorff, 1995; Wunder and Schreyer, 1997; Padrón-Navarta et al., 2010b), In addition, the occurrence of tremolite in the Chl-harzburgites limits the maximum temperature from 680 to 710 °C for 1.9 and 1.6 GPa, respectively (Padrón-Navarta et al., 2010b). These P-T conditions compare well with independent estimates for metarodingite (1.6-1.9 GPa and 660-684 °C; Laborda-López et al., 2018) and ophicarbonate lenses hosted within the Chl-harzburgites (18 kbar, 650–670 °C; Menzel et al., 2019). These studies suggest that the peak metamorphic conditions experienced by the Cerro del Almirez massif were 680–710 °C and 1.6–1.9 GPa, notably high in temperature for a given pressure as compared to other alpine meta-ophiolites (Fig. 2).

In the massif, the transition from Atg-serpentinites to Chl-harzburgites is marked by a sharp increase in the abundance of olivine, orthopyroxene and chlorite concomitant with a steady disappearance of antigorite (Padrón-Navarta et al., 2011). In the field, the transition from Atg-serpentinites to Chl-harzburgites takes place over few meters (< 2 m) where serpentinites are composed of Atg + Chl + Ol ± Opx and correspond to partly dehydrated serpentinites that have been termed "transitional" lithologies in previous studies (Padrón-Navarta et al., 2011). The contact between Atg-serpentinites and transitional lithologies developed obliquely to the foliation of the Atg-serpentinite and shows no signs of tectonic activity or offset. In addition to the Atg-serpentinite, Chl-harzburgite and transitional lithologies, the massif also contains minor metarodingite boudins and ophicarbonates lenses that, together with the Atg-serpentinites, preserve a textural and geochemical record of seafloor serpentinization and carbonation processes (Alt et al., 2012; Laborda-López et al., 2018; Menzel et al., 2019), which likely took place during the opening of the western branch of the Alpine Tethys Ocean in the Mesozoic (Puga et al., 2011).

In this study, we selected samples from the three distinctive lithologies from the Cerro del Almirez massif: Atg-serpentinites, transitional lithologies, and Chl-harzburgites with granofels, spinifex and recrystallized textures (Table 1). In order to evaluate the potential contribution of sediment-derived external fluids, we also analyzed two metasedimentary mica-schists surrounding the Cerro del Almirez massif.

3. Methodology

Whole rock powders were dissolved using concentrated HF and HNO_3 acids in 7 mL PTFE Teflon square digestion vessels with wrench top closures in an oven at 160 °C for 3 days. Following evaporation of the HF and HNO_3 the samples were subsequently treated with a 1:1 mix of concentrated HCl and HNO_3 and refluxed at 140 °C for 3 days in an oven. Prior studies comparing this method to Parr-bomb dissolution techniques (Debret et al., 2018) have shown that it can digest all refractory phases that may be present in serpentinites, including spinel (see Results section for further discussion). Finally, samples were brought into solution in 6 M HCl and 1.5 M HBr before Fe and Zn column chemistry, respectively. Quantitative purification of Fe was achieved by chromatographic exchange, using Biorad AG1-X4 anion exchange resin

in an HCl medium following the procedure of Williams and Bizimis (2014). The quantitative separation of Zn from matrix elements was achieved using Teflon shrink-fit columns filled with 0.5 mL of Biorad AG1-X4 anion exchange resin following the procedure adapted from Moynier et al. (2006). All reagents used in the chemistry and mass spectrometry procedures were distilled in sub-boiling Teflon two-bottle stills at Durham University (UK), except for the HBr acid, which was ultra-pure grade ROMIL grade. The total amount of Fe and Zn processed through the columns was typically around 650 µg and 1250 ng, respectively. The total procedural blank contribution was <50 ng of Fe and <10 ng of Zn, which is negligible compared to the amount of Fe and Zn in the samples.

Iron and Zn isotope analyses were performed by multiple-collector inductively coupled plasma mass spectrometry (MC-ICP-MS; Thermo Scientific Neptune Plus) at Durham University (UK). Instrumental mass fractionation was corrected using the sample-standard bracketing technique for Fe, and combined sample-standard bracketing and external empirical normalisation with a Cu standard for Zn (e.g., Maréchal et al., 1999). In the case of Fe analyses, solutions consisted of 2 ppm natural Fe in 0.1 M HNO_3, which were introduced into the mass spectrometer using a quartz SIS (stable introduction system; ThermoFisher) and PFA 50 µl/min nebuliser. The international Fe isotope standard IRMM014 was used as both the bracketing and delta notation reporting standard. To resolve the polyatomic interferences $^{40}Ar^{16}O$, $^{40}Ar^{14}N$, and $^{40}Ar^{16}OH^+$ that occur on masses ^{56}Fe, ^{54}Fe, and ^{57}Fe, respectively, the instrument was run in medium resolution mode, which gave a mass resolving power (mass/Δmass) of ~8000. The standard Fe beam intensities typically varied between 25 and 35 V for ^{56}Fe using a 10^{10} Ω resistor. Data were collected in 25 cycles of 4.194 second integrations. Mass dependence, long-term reproducibility, and accuracy were evaluated by analyzing an in-house $FeCl_2^-$ salt standard. The values obtained for repeated measurements of this standard solution yielded average $\delta^{56}Fe$ values of −0.70 ±0.05 ‰ and $\delta^{57}Fe$ values of −1.03 ±0.09 ‰ 2sd, n =24. These average values are in excellent agreement with previous measurements (Williams and Bizimis, 2014). The international rock reference material USGS BIR-1a (Icelandic basalt) was analyzed in

the same analytical sessions as the samples, yielding $\delta^{56}Fe$ values of 0.06 ± 0.02 ‰ and $\delta^{57}Fe$ = 0.08 ± 0.01 ‰ (2sd, *n* = 2; see appendix A).

Zinc isotope compositions were measured on the purified sample solutions. These solutions were prepared at 750 ng/g of natural Zn and doped with 250 ng/g of pure Cu solution. This gave a Zn intensity of ~ 4V for ^{64}Zn. The solutions were introduced to the instrument using a PFA 50 µl/min nebuliser coupled to a quartz cyclonic spray chamber. Owing to a lack of polyatomic interferences across the mass range for Zn the machine was operated in low mass resolution mode. Mass of ^{62}Ni was monitored to correct for the potential interference of ^{64}Ni on ^{64}Zn. Data were collected in 40 cycles of 4.194 second integrations. Because the widely used Zn isotope standard (JMC-Lyon) is exhausted, an in-house pure Zn solution obtained from Alfa-Asear was used as the bracketing standard. This standard solution was calibrated relative to the JMC-Lyon solution, and an offset for $\delta^{66}Zn$ of +0.28‰ was observed. This allowed for the measured $\delta^{66}Zn_{Alfa\text{-}Asear}$ to be corrected to $\delta^{66}Zn_{JMC\text{-}Lyon}$ by applying a correction value of +0.28‰ to all values. The mass dependence, long-term reproducibility and accuracy of this method were evaluated by the analysis of the external reference material USGS BHVO-2, which yielded a $\delta^{66}Zn$ value of 0.35 ± 0.05 ‰ (2sd, *n* = 2). This value is in excellent agreement with previously published values (see appendix A).

4. Results

Iron and zinc isotopic ratios were measured in the Cerro del Almirez samples and given in Table 1. Major and trace element data, including iron and zinc concentrations, are from Marchesi et al. (2013). The $\delta^{56}Fe$ values of Cerro del Almirez rocks range from -0.06 ± 0.04 ‰ to +0.12 ± 0.04 ‰ with a mean $\delta^{56}Fe$ value of +0.05 ± 0.02 ‰ (2sd/√n; n = 24), comparable to that of the primitive mantle (+0.03 ± 0.03 ‰; Craddock et al., 2013; Poitrasson et al., 2013; Sossi et al., 2016; Fig. 3a). Among Cerro del Almirez samples, Chl-harzburgites display a larger range of $\delta^{56}Fe$ (from -0.06 ± 0.04 to +0.09 ± 0.03 ‰) relative to Atg-serpentinites (+0.01 ± 0.01 to +0.10 ± 0.03 ‰) and transitional lithologies (+0.00 ± 0.01 to +0.08 ± 0.01 ‰). The mean value of Chl-harzburgites decreases from granofels (+0.07 ± 0.02 ‰, 2sd/√n; n = 4) to spinifex (+0.04 ± 0.03 ‰, n = 5) and recrystallized textures (-0.01 ± 0.05 ‰, n = 3; Fig. 3a). The FeO

contents of these samples range from 6.7 to 8.7 wt% and are indistinguishable from those observed in abyssal and orogenic serpentinites (e.g., Deschamps et al., 2013).

Zinc concentrations [Zn] and isotope ratios ($\delta^{66}Zn$) range broadly from 34 to 74 ppm and from +0.09 to +0.55 ‰, respectively. The [Zn] and $\delta^{66}Zn$ values of Cerro del Almirez samples are generally higher than those assumed for the primitive mantle ([Zn] = 55 ppm; mean $\delta^{66}Zn$ = +0.16 ± 0.06 ‰; Sossi et al., 2018). Given that spinels commonly display high [Zn] and $\delta^{66}Zn$ values relative to mantle silicates and sulfides (Wang et al., 2017; Ducher et al., 2016), the incomplete dissolution of spinel in our samples cannot explain these variations as this should lead to apparently lighter $\delta^{66}Zn$ and low [Zn] relative to mantle values. The $\delta^{66}Zn$ values observed in our samples increase from Atg-serpentinites ([Zn] = 34–46 ppm; $\delta^{66}Zn$ = +0.23 ± 0.06‰), to transitional lithologies (Zn = 45–67 ppm; $\delta^{66}Zn$ = +0.30 ± 0.06‰), granofels ([Zn] = 38–59 ppm; $\delta^{66}Zn$ = +0.33 ± 0.04‰) and spinifex ([Zn] = 48–66 ppm; $\delta^{66}Zn$ = +0.43 ± 0.09‰) Chl-harzburgites (Fig. 3b). The recrystallized Chl-harzburgites display scattered $\delta^{66}Zn$ values (from +0.21 ± 0.04 ‰ to +0.49 ± 0.03 ‰) with a mean of +0.33 ± 0.12‰. Two samples of the mica-schists surrounding the Cerro del Almirez massif were also analyzed. They are characterized by similar FeO (6.44 and 8.26 wt%) and $\delta^{56}Fe$ (+0.05 ± 0.02 and +0.11 ± 0.02 ‰) and high [Zn] (113 and 125 ppm) and $\delta^{66}Zn$ (+0.33 ± 0.04 and +0.46 ± 0.03 ‰) compared with meta-serpentinites (i.e., the Atg-serpentinites, transitional lithologies, granofels, spinifex and recrystallized -textured Chl-harzburgites).

5. Discussion

Serpentinites are significant reservoirs of water and redox-sensitive elements (e.g., Alt et al., 2013). Their high-pressure dehydration to meta-peridotite at depth in subductions zones is the main source of water for arc magmatism, triggers large scale metasomatism of the mantle wedge area, and influences redox sensitive element cycles between the Earth's interior and surface (Debret and Sverjensky, 2017; Cannao and Malaspina, 2018; Iacovino et al., 2020; Menzel et al., 2020). The subduction-related Cerro del Almirez complex provides an unmatched opportunity to investigates these processes because this is the only exhumed massif worldwide that preserves a reaction front between Atg-serpentinites and their high-pressure

dehydration product, Chl-harzburgites (Trommsdorff et al., 1998; Padrón-Navarta et al., 2011; Alt et al., 2012; Marchesi et al., 2013).

Before addressing the significance of the Cerro del Almirez Fe and Zn stable isotope data in the context of high-pressure dehydration of serpentinite in subduction zones, it is essential to first investigate the effects of high temperature petrogenetic processes and seafloor hydrothermal alteration that may have modified the oceanic lithosphere prior to subduction. The major, trace element and stable isotope composition of the oceanic mantle lithosphere is influenced by high temperature melting and melt extraction processes, which ultimately define its "fertility" (*i.e.*, the degree to which mantle peridotite has experienced prior melt extraction and its capacity to produce partial melts). To explore how these processes could have influenced Fe and Zn isotope systematics we need to evaluate potential correlations between $\delta^{66}Zn$, $\delta^{56}Fe$ and chemical indicators of mantle fertility. The degree of mantle peridotite fertility is manifested in the modal abundances of pyroxenes and hence can be qualitatively estimated using Al_2O_3 contents, with fertile lherzolites displaying high Al_2O_3 relative to refractory harzburgites and dunites (e.g., Bodinier and Godard, 2013). In serpentinites Al_2O_3/SiO_2 is considered a better proxy of peridotite protolith composition than Al_2O_3 concentrations because the Al_2O_3/SiO_2 ratio remains relatively unchanged during the serpentinization process, whereas Al_2O_3 concentrations can be influenced by volume changes accompanying serpentinite formation (see Paulick et al., 2006; Deschamps et al., 2013). Although serpentinite bulk-rock MgO values can retain some magmatic signals (Niu, 2004), serpentinized peridotites mostly display MgO/SiO_2 ratios that mostly fall below the terrestrial mantle array (Figure 4a). Previous authors have attributed this observation to a loss of MgO during low temperature seafloor weathering (e.g., Snow and Dick, 1995; Niu, 2004; Paulick et al., 2006; Deschamps et al., 2013). In the following discussion we therefore use the Al_2O_3/SiO_2 ratio instead of Al_2O_3, MgO contents or MgO/SiO_2 to quantify fertility variations in Cerro del Almirez protolith(s).

Previous studies have shown that the $\delta^{56}Fe$ values of peridotites can be highly influenced by melt extraction, with higher $\delta^{56}Fe$ preserved in lherzolites relative to harzburgites and dunites (Williams et al., 2005; Weyer

and Ionov, 2007), where the latter display light $\delta^{56}Fe$ as a consequence of losing isotopically heavy Fe to a melt phase. The range in $\delta^{56}Fe$ (-0.06–0.12 ‰) and the Al_2O_3/SiO_2 (0.03–0.09) ratios observed in the Cerro del Almirez samples are comparable to those of mantle peridotites and abyssal serpentinites ($\delta^{56}Fe$ -0.14–+0.08 ‰; Debret et al., 2018a; Al_2O_3/SiO_2 = 0.01–0.09; Godard et al., 2008) and a broad correlation between Al_2O_3/SiO_2 and $\delta^{56}Fe$ is observed (Fig. 4b). These observations suggest that the $\delta^{56}Fe$ variations of Cerro del Almirez samples are mainly controlled by peridotite protolith $\delta^{56}Fe$ compositions, which in turn may record prior melt extraction and/or refertilisation processes.

In contrast to Fe, there are significant variations in the Zn isotope compositions of the Cerro del Almirez samples (+0.09 ± 0.02 ‰ to +0.55 ± 0.09 ‰; Fig. 3), which are well resolved from primitive mantle values (+0.16 ± 0.06 ‰; Sossi et al., 2018). The absence of any correlations between $\delta^{66}Zn$ and indices of fertility such as Al_2O_3/SiO_2 (Fig. 4c) suggests that the Zn isotope compositions of the Cerro del Almirez samples have been overprinted by subsequent metamorphic processes, taking place during either oceanic stage serpentinisation or prograde subduction related metamorphism. In a recent study, Bretscher et al. (2018) speculated that the Atg-out reaction front between the Cerro del Almirez Chl-harzburgites and Atg-serpentinites may correspond to a sharp oxidation seafloor serpentinization front, with the Chl-harzburgite protolith representing the deep part of the oceanic lithosphere and the Atg-serpentinite protolith formed at shallower depths. In the scenario proposed by Bretscher et al. (2018), abyssal serpentinization processes control the contrasting mineralogical and chemical variations observed across the contact between Atg-serpentinites and Chl-harzburgites in the Cerro del Almirez, rather than prograde subduction-related metamorphism and devolatilisation processes (Padrón-Navarta et al., 2011).

These scenarios can be distinguished using Zn stable isotopes. Abyssal peridotites and serpentinites display a large range of $\delta^{66}Zn$ (from 0.13‰ to 0.47‰), with highly serpentinized peridotites displaying low [Zn] and high $\delta^{66}Zn$ relative to fresh mantle peridotites (Fig. 5a; Debret et al., 2018a). Debret et al., (2018a) attributed these variations to the preferential mobility and loss of isotopically light Zn in fluids during abyssal serpentinization, with Zn stable isotope fractionation being controlled by the dissolution of both

mantle sulfides and/or spinels and Zn complexation with chlorine in fluids. In the Cerro del Almirez massif, transitional lithologies ($\delta^{66}Zn$ = +0.30 ± 0.06‰) granofels ($\delta^{66}Zn$ = +0.33 ± 0.04‰) and spinifex ($\delta^{66}Zn$ = +0.43 ± 0.09‰) Chl-harzburgites display higher $\delta^{66}Zn$ values relative to Atg-serpentinites ($\delta^{66}Zn$ = +0.23 ± 0.06‰), as showed by a broad negative correlation between $\delta^{66}Zn$ and Loss On Ignition (LOI, a broad measure of the presence of hydrous phases such as serpentine) values (Fig. 5b). Furthermore, the studied Chl-harzburgites display high [Zn] (38-74 ppm) relative to abyssal peridotites and serpentinites (29-45 ppm, Debret et al., 2018a; Fig. 5) and a broad positive correlation is observed between $\delta^{66}Zn$ and [Zn] (Fig. 5a). These results contrast with previous observations in abyssal settings, where negative correlation between $\delta^{66}Zn$ and [Zn] was interpreted as reflecting spinel dissolution during peridotite serpentinization and Zn leaching in hydrothermal fluids (Fig. 5; see also Debret et al., 2018a). This comparison demonstrates that the observed variations in the Cerro del Almirez meta-serpentinites cannot be explained by differences in the degree of seafloor serpentinization (c.f. Bretscher et al., 2018). Instead, the Zn elemental and isotopic variations observed in the Cerro del Almirez massif are most likely to reflect the mobility of Zn in metamorphic fluids at high pressures and temperatures during the progressive dehydration of Atg-serpentinites into transitional lithologies and Chl-harzburgites. The observed Zn isotope fractionation can therefore be used to place constraints on the composition of slab derived fluids during subduction, as we discuss in detail below.

Zinc isotope fractionation is highly influenced by the (re-)crystallization of Fe-oxides (e.g., spinels), sulfides and carbonates, which are the main carriers of Zn in ultramafic rocks (e.g., Wang et al., 2017; Debret et al., 2018a). The subduction of the oceanic lithosphere initiates a continuum of metamorphic redox reactions and dehydration/rehydration events between the downgoing slab and the slab/mantle wedge interface and/or the mantle wedge that influence Fe-oxides, sulfides and carbonates stability resulting in stable isotope fractionation (Debret et al., 2016). The Zn concentration and isotope composition of the Cerro del Almirez Atg-serpentinites are consistent with those observed in other high-P slab serpentinites, such as those from the Western Alps meta-ophiolites (Pons et al., 2016) (Fig. 5a). However, in contrast to the Western Alps, in

the Cerro del Almirez massif the dehydration of Atg-serpentinites to prograde Chl-harzburgites is accompanied by an increase in both bulk rock δ^{66}Zn values and [Zn] (Fig. 5). Furthermore, the metamorphic recrystallization of Atg-serpentinites into Chl-harzburgites is accompanied by a decrease of magnetite modal abundance in bulk rock (Debret et al., 2015), suggesting a change in serpentinite redox budget during subduction. One possible explanation for these observations is the dissolution of Zn-bearing spinels and the subsequent leaching of isotopically heavy Zn in metamorphic fluids during serpentinites dehydration. However, Fe-oxides tend to display high δ^{66}Zn and [Zn] concentrations relative to silicates (Ducher et al., 2016; Wang et al., 2017), suggesting this scenario is unlikely.

Another possibility is that Zn stable isotope variations in the Cerro del Almirez meta-serpentinites were produced by the influx of external fluids (i.e., open-system processes), rather than by the *in situ* (closed-system) dehydration of serpentinites during subduction. Recent studies show that Zn can be highly mobile in slab derived fluids forming carbonate (e.g., Zn–CO_3) and/or sulfate (e.g., Zn–SO_4) aqueous complexes, and that these preferentially complex isotopically heavy Zn relative to silicates, Fe-oxides, sulfides and/or carbonates (Fuji et al., 2014; Liu et al., 2016; Pons et al., 2016; Ducher et al., 2016; Debret et al., 2018b). The elevated δ^{66}Zn values and Zn concentrations of the Cerro del Almirez Chl-harzburgites relative to those of Atg-serpentinites (Figs 3 and 5) may therefore be interpreted in terms of the dehydration of Atg-serpentinite in conjunction with the influx of external fluids with heavy Zn isotope signatures, such as those released during slab devolatilization (Liu et al., 2016; Pons et al., 2016; Debret et al., 2018b).

Previous geochemical studies have shown that the Cerro del Almirez Chl-harzburgites are abnormally enriched in Th, U, Nb, Ta, Pb, large ion lithophile elements (LILE, Cs, Rb, Ba, Sr) and light δ^{11}B relative to Atg-serpentinites (Garrido et al., 2005; Marchesi et al., 2013; Harvey et al., 2014). These enrichments cannot be explained by closed-system dehydration of serpentinite (Marchesi et al., 2013). Furthermore, these geochemical characteristics (i.e., LILE, Sr and B enrichments) are also shared with fluid inclusions trapped in metamorphic olivine and orthopyroxene from Chl-harzburgites (Scambelluri et al., 2004a, b), providing strong evidence for the equilibration of the Chl-harzburgites with a fluid phase enriched in these

elements. Taken together, these observations show that dehydration must have occurred in an open system involving external fluids that equilibrated with other lithologies such as metasedimentary rocks (Jabaloy et al., 2015), meta-rodingites (Laborda-López et al., 2018), meta-ophicarbonates (Menzel et al., 2019), and/or an exotic slab-derived component (Marchesi et al., 2013; Harvey et al., 2014). Interestingly, the Cerro del Almirez samples display broad positive arrays between δ^{66}Zn and Sr/Y, Ba/Ce or Rb/Ce ratios with the Chl-harzburgites displaying high δ^{66}Zn, Sr/Y, Ba/Ce and Rb/Ce ratios relative to the other lithologies as well as higher and more variable U/Yb ratios (Fig. 6). Similarly, the metasedimentary rocks also display high δ^{66}Zn, Sr/Y, U/Yb, Ba/Ce and Rb/Ce and plot in the same area as the Chl-harzburgites in Fig. 6.

The mean δ^{66}Zn of clastic sediments is +0.28 ± 0.13 ‰ (n = 105; Moynier et al., 2017) and is highly influenced by the presence of carbon, sulfur and iron-bearing phases, which typically display isotopically heavy signatures relative to silicate-bearing minerals (Fujii et al., 2014; Ducher et al., 2016). The Zn isotope signatures of micaschists (+0.33 ± 0.04 and +0.46 ± 0.03 ‰) surrounding the Cerro del Almirez ultramafic massif are extremely similar to the clastic sediment mean value, such that it is difficult to estimate the magnitude and direction of any Zn stable isotope fractionation that may take place during the high-P dehydration of these sedimentary rocks. However, given the similarity in micaschist and Chl-harzburgite δ^{66}Zn values and the observation that Cerro del Almirez metasedimentary rocks also display high [Zn] (113–125 ppm), it is plausible to consider that fluids in equilibrium with the micaschists could, at the very least, have inherited their heavy δ^{66}Zn signatures. Infiltration of the the Chl-harzburgites with such heavy- δ^{66}Zn sediment-derived fluids could thus have modified their Zn isotope signatures, explaining the heavy δ^{66}Zn values observed. Furthermore, the devolatilization of metasedimentary rocks at high pressures is likely to release carbon-bearing fluids due to carbonate devolatilization (e.g., Debret et al., 2018b). Given that these aqueous complexes preferentially incorporate heavy Zn isotopes (Fuji et al.,2014) relative to Zn-bearing Fe-oxides, sulfides or carbonates (Ducher et al., 2016), the fluids derived from metasedimentary rocks could be even more fractionated to even heavier δ^{66}Zn values than the sedimentary (micaschist) residues from which they were derived.

The recent study of Ferrando et al. (2019) on high-pressure fluid inclusions in kyanite reveals that the progressive dissolution of phengite and carbonate in metasedimentary rocks results in the preferential release of LILE, U, Th and Sr to a fluid phase. The fluid inclusions in the Chl-harzburgites display similar anomalies in LILE and Sr (Scambelluri et al., 2004a, b) to those described by Ferrando et al. (2019), reinforcing the idea of a sediment-derived fluid input to the Cerro del Almirez meta-serpentinites. Similarly, the high F contents and $^{20}Ne/^{36}Ar$ ratios of the Cerro del Almirez Chl-harzburgites have been ascribed to the open-system influx of F^-, ^{40}Ar, ^4He- and ^{20}Ne-rich fluids derived from metasedimentary rocks (Kendrick et al., 2018). Hence, we suggest that the heavy Zn isotope composition of Chl-harzburgites, as well as their trace element compositions, is consistent with metasomatism by carbonate-bearing fluids derived from the metasedimentary rocks. This hypothesis is also in agreement with the observation of Mg-carbonates associated with high-pressure minerals in Cerro del Almirez Chl-harzburgites (Menzel et al., 2019), those being commonly interpreted as subduction related (e.g., Scambelluri et al., 2016).

In order to further test this hypothesis, we first attempted to model the Zn isotope composition of carbon bearing fluids released during sediment dehydration at HP. Carbon can exist in deep fluids as either carbonate and/or organic molecules, which can be stable, at low oxygen fugacity and/or pH, up to 6 GPa and more than 600 °C in subduction zones (Sverjensky et al., 2014). We therefore considered both carbonate [$ZnCO_3(H_2O)_3$, $ZnHCO_3(H_2O)^{5+}$] and organic carbon [$Zn(cit)_2^{4-}$] as potential complexes for Zn in metasediment derived fluids. These different carbon-bearing species were chosen based on their different partition functions, or β-factors, and contrasting oxidation state of carbon. The influence of organic ligands on Zn isotope partitioning was approximated by using citrate as a representative ligand in our calculations; moreover, no other *ab initio* calculation results are currently available for other organic complexes, such as acetate (see review in Moynier et al., 2017), which are potentially more representative of subduction-zone fluids (Sverjensky et al., 2014). Using these, the compositions of the Chl-harzburgites was modelled in the form of a binary mixture between metasediment-derived fluids and Atg-serpentinites. The elemental and isotopic behaviour of Zn in carbonate-bearing metasedimentary rocks (i.e., the β-factor) was approximated

to that of smithsonite ($ZnCO_3$). We used the *ab initio* calculations of Fujii and Albarède (2012) and Moynier et al. (2017) for [$ZnHCO_3(H_2O)^{5+}$, $Zn(cit)_2^{4-}$] and [$ZnCO_3(H_2O)_3$] complexes in fluids and those of Ducher et al. (2016) for smithsonite. The $\delta^{66}Zn$ composition of the metasediment derived fluids was modelled using a simple Rayleigh distillation law, according to the following equations:

$$10^3 \ln(\alpha_{fluid\text{-}mineral}) = 10^3 \ln(\beta_{fluid}) - 10^3 \ln(\beta_{mineral})$$

$$\delta^{66}Zn_{Final} = (1000 + \delta^{66}Zn_{Initial}) \times (F^{(\alpha-1)} - 1) + \delta^{66}Zn_{Initial}$$

where α is the fractionation factor between smithsonite and a fluid phase complexing Zn as [$ZnHCO_3(H_2O)^{5+}$], [$ZnCO_3(H_2O)_3$] or [$Zn(cit)_2^{4-}$] at temperatures ranging from 500 to 700 °C. *F* is the fraction of Zn remaining in the rock, ranging from 1 (unreacted) to 0 (all of Zn lost to the fluid phase). As we expect the mobility of Zn to be low in metasediment-derived fluids (see discussion above), we set F to be 0.9 in our models. The $\delta^{66}Zn_{Initial}$ was set to 0.4 ‰, which is the mean value of countryside metasedimentary rocks surrounding the Cerro del Almirez massif. The composition of the Cerro del Almirez samples was then modelled as a binary mixture between Atg-serpentinites and metasediment-derived fluids according to the following equation:

$$\delta^{66}Zn_{mixture} = (N_a\delta^{66}Zn_a + N_b\delta^{66}Zn_b) / (N_a + N_b)$$

where N_a and N_b are the amounts of Zn transported by fluids and the initial abundance of Zn in Atg-serpentinites, respectively. The results of these models are plotted in Figure 7 and serves to demonstrate that the high [Zn] and $\delta^{66}Zn$ of Cerro del Almirez Chl-harzburgites is consistent with the percolation of [$ZnHCO_3(H_2O)^{5+}$] and [$ZnCO_3(H_2O)_3$] fluids at temperatures ranging from 500 °C to 700 °C.

Our models can also be used to explore the effect of reduced carbon species in fluids, such organic carbon (illustrated on Figure 7 as citrate), on Zn isotope systematics and to determine whether percolation by such fluids can explain the $\delta^{66}Zn$ variation in the Chl-harzburgites. However, reduced carbon species do not fractionate Zn isotopes to the extent that they can create fluids with sufficiently heavy $\delta^{66}Zn$. Models using available data for Zn isotope partitioning into such fluids were not able to reproduce the observed $\delta^{66}Zn$

variations in the Chl-harzburgites (Fig. 7). These observations are consistent with presence of titano-hematite in Chl-harzburgites, which is a phase expected to crystallize at relatively high oxygen fugacities (between +1 and +4 relative to quartz-fayalite-magnetite buffer), under which carbon is stable under oxidized form (Debret et al., 2015; Debret and Sverjensky, 2017). Furthermore, recent studies and thermodynamic modelling of Cerro del Almirez meta-ophicalcites indicate that both CO_2 and HCO_3^- species are likely to dominate fluids circulating in the massif during antigorite breakdown (Menzel et al., 2020), in agreement with our hypothesis.

The geochemical imprint of metasediment-derived fluids also occurs in other subduction-related Chl-harzburgites. This is seen in Western Alps meta-ophiolites (Fig. 2), such as the Cima di Gagnone (Lepontine Alps) and Erro Tobbio (Scambelluri et al., 2019; Cannao et al., 2020). These observations point to a widespread association between open-system dehydration processes and oxidized fluids conditions (*i.e.*, associated carbonate- or sulfate-bearing fluids). Such processes may therefore be ubiquitous in subduction zones, particularly near the slab-wedge interface, where serpentinites are continuously percolated by fluids with sediment-like signatures.

Long-range and large-scale fluid flows, such as the migration of slab derived fluids to the mantle wedge, are known to occur in subduction zones. Although the sources and compositions of fluids in subduction zones are expected to be highly variable, recent studies have proposed that fluids circulating in subduction zones are likely to display fractionated Zn and/or Fe isotopes signatures (Debret et al., 2016; Pons et al., 2016; Debret et al., 2018b; Gerrits et al., 2019; Chen et al., 2019; Liu and Li, 2019). In particular, the observation of high $\delta^{66}Zn$ in Chl-harzburgites is consistent with the results of previous studies showing that isotopically heavy Zn is likely to be mobile during carbonate dissolution at high pressure in subduction zones (Liu et al., 2016; Debret et al., 2018b; Liu and Li, 2019). However, the lack of significant Fe isotope variation in the Cerro del Almirez samples is surprising as isotopically light Fe is also expected to be mobile in carbonate-bearing fluids (Fujii et al., 2014). Indeed, previous studies working in forearc mantle wedge or shallow slab/mantle interface areas have shown that large Fe isotope variations in ultramafic rocks (down

to -0.26 ‰) may be attributed to carbonate-bearing metasomatism (Inglis et al., 2017; Debret et al., 2018b, 2020) and the dissolution of Ca- (i.e., calcites, aragonite) and/or Fe- (i.e., siderite and ankerite) bearing carbonates in metamorphic fluids at low temperature (i.e., below 400 °C; Facq et al., 2014; Milesi et al., 2015). Both Ca- (down to -0.92 ‰; Craddock and Dauphas, 2011) and Fe- (down to -3.9 ‰; Belshaw et al., 2000; Johnson et al., 2008) bearing seafloor carbonates are known to concentrate isotopically light Fe relative to silicate and oxide phases. However, in contrast to Ca-/Fe- carbonates, Mg-rich carbonates (e.g., magnesite) are comparatively insoluble at low pressures and become progressively soluble in water with increasing pressure and temperature (e.g., Pan et al., 2013). It is therefore possible that the sequential dissolution of Ca- /Fe- bearing carbonates to Mg- bearing carbonates during slab burial could generate carbonate-bearing fluids with a spectrum of Zn and Fe isotope signatures, with shallow fluids resulting from Ca- and Fe- bearing carbonate dissolution displaying isotopically light Fe signatures, and deep fluids resulting from Mg-carbonate dissolution displaying isotopically heavy Zn isotope compositions. This hypothesis is also consistent with the low Fe content of magnesite, such that the dissolution of these carbonates and the low-Fe fluids released will not significantly impact the Fe isotope compositions of carbonated mantle peridotites. Interestingly, the recent study of Shen et al. (2018) reported light $\delta^{26}Mg$ values for deep mantle wedge peridotites from the Dabie orogen (5.3-6.3 GPa; 800 °C) that were interpreted as evidence for the dissolution and transfer of sedimentary Mg-rich carbonate by supercritical fluids at sub-arc depths (~160km), a scenario consistent with our observations from the Cerro del Almirez massif.

6. Conclusion

Our study results demonstrate the decoupled nature of the Fe and Zn isotope variations in Cerro del Almirez meta-serpentinites. The $\delta^{56}Fe$ variations of ultramafic rocks are compatible with a mantle signature, as shown by covariations between $\delta^{56}Fe$ and indices of melt extraction (i.e., Al_2O_3/SiO_2). The $\delta^{66}Zn$ and Zn concentrations of the Atg-serpentinites are similar to those of slab derived serpentinites from high-pressure meta-ophiolites. However, the Chl-harzburgites are abnormally enriched in isotopically heavy Zn that is accompanied with an increase of Zn concentrations and Sr/Y, U/Yb, Ba/Ce and Rb/Ce ratios. These

observations are concordant with the percolation of external carbon-bearing fluids enriched in isotopically heavy Zn. Geochemical models show that Zn isotope fractionation could be driven by [$ZnHCO_3(H_2O)^{5+}$] and [$ZnCO_3(H_2O)_3$] complexes in metamorphic fluids at temperatures ranging from 500 °C to 700 °C. Our models show that reduced carbon species cannot reproduce the observed $\delta^{66}Zn$ variations in the massif. We conclude that the decoupling behavior of Fe and Zn during Chl-harzburgite metasomatism is consistent with the dissolution and mobility of Mg-(Zn)-rich and Fe-poor carbonates in oxidizing fluids at high pressures during subduction.

AKNOWLEDGMENT

We thank G. Nowell (Durham University, UK) for technical support and K. Burton (Durham University, UK) for fruitful discussions. This work was supported by a Natural Environment Research Council (NERC) Deep Volatiles Consortium Grant (NE/M000303/1), a European Research Council (ERC) Starting Grant (HabitablePlanet; 306655) to H. Williams, and by the TelluS Program of CNRS/INSU. B Debret acknowledges financial support by LabEx UnivEarthS (ANR-10-LABX-0023 and ANR-18-IDEX-0001). M. T. Gómez-Pugnaire, J. A. Padrón-Navarta, and C. Marchesi are thanked for early work and characterization of the samples investigated in the present study. We are grateful to the Sierra Nevada National Park authorities for providing the permit for fieldwork and sampling at the Cerro del Almirez massif. E.I. is supported as a postdoc on an ERC Horizon 2020 advanced grant (SHRED; 833632) awarded to Dr. C. Chauvel (IPG, Paris). C.J.G. and V.L.S.-V. acknowledge funding from the "Spanish Ministry of Science and Innovation" and "Agencia Estatal de Investigación (AEI)" grants no. CGL2016-75224-R and CGL2016-81085-R, and from the "Junta de Andalucía" research group grants RNM-131 and RNM-374. We thank S.-A. Liu, R. Halama and two anonymous reviewers for critical comments on earlier version of this article and careful editorial handling by D.A. Ionov.

REFERENCES

Agard P., Jolivet L. and Goffé B. (2001) Tectonometamorphic evolution of the Schistes Lustrés complex: implications for the exhumation of HP and UHP rocks in the Western Alps. *Bull. Soc. Geol. Fr.* **172**, 617-636

Alt J. C., Garrido C. J., Shanks W. C., Turchyn A., Padrón-Navarta J. A., López Sánchez-Vizcaíno V., Gómez Pugnaire M. T. and Marchesi C. (2012) Recycling of water, carbon, and sulfur during subduction of serpentinites: A stable isotope study of Cerro del Almirez, Spain. *Earth Planet. Sci. Lett.* **327**–**328**, 50–60. 10.1016/j.epsl.2012.01.029.

Alt J. C., Schwarzenbach E. M., Früh-green G. L., Shanks W. C., Bernasconi S. M., Garrido C. J., Crispini L., Gaggero L., Padrón-Navarta J. A. and Marchesi C. (2013) The role of serpentinites in cycling of carbon and sulfur : Seafloor serpentinization and subduction metamorphism. *Lithos* **178**, 40–54. 10.1016/j.lithos.2012.12.006.

Behr, W.M., Platt, J.P., (2012) Kinematic and thermal evolution during two-stage exhumation of a Mediterranean subduction complex. *Tectonics* **31**. 10.1029/2012tc003121.

Belshaw, N. S., Zhu, X. K., Guo, Y. & O'Nions, R. K. (2000) High precision measurement of iron isotopes by plasma source mass spectrometry. *International Journal of Mass Spectrometry* **197**, 191–195.

Bodinier J. L. and Godard M. (2013) *Orogenic, Ophiolitic, and Abyssal Peridotites*. 3rd ed., Elsevier Ltd. http://dx.doi.org/10.1016/B978-0-08-095975-7.00204-7.

Booth-Rea, G., Martínez-Martínez J., and Giaconia F. (2015) Continental subduction, intracrustal shortening, and coeval upper-crustal extension: PT evolution of subducted south Iberian paleomargin metapelites (Betics, SE Spain). *Tectonophysics* **663**, 122–139.

Bretscher A., Hermann J. and Pettke T. (2018) The influence of oceanic oxidation on serpentinite dehydration during subduction. *Earth Planet. Sci. Lett.* **499**, 173–184. 10.1016/j.epsl.2018.07.017.

Cannaò E. and Malaspina N. (2018) From oceanic to continental subduction: Implications for the geochemical and redox evolution of the supra-subduction mantle. *Geosphere* **14**, 2311–2336.

Cannaò E., Tiepolo M., Bebout G. E. and Scambelluri M. (2020) Into the deep and beyond : Carbon and nitrogen subduction recycling in secondary peridotites. *Earth Planet. Sci. Lett.* **543**, 116328.

Chen, Y.X., Lu, W., He., Y., Schertl, H.P., Zheng, Y.F., Xiong, J.W. and Zhou K. (2019). Tracking Fe mobility and Fe speciation in subduction zone fluids at the slab-mantle interface in a subduction channel: A tale of whiteschist from the Western Alps. *Geochim. Cosmochim. Acta* **267**, 1–16.

Craddock P. R., Warren J. M. and Dauphas N. (2013) Abyssal peridotites reveal the near-chondritic Fe isotopic composition of the Earth. *Earth Planet. Sci. Lett.* **365**, 63–76. 10.1016/j.epsl.2013.01.011.

Dauphas N., Roskosz M., Alp E., Golden D., Sio C., Tissot F., Hu M., Zhao J., Gao L. and Morris R. (2012) A general moment NRIXS approach to the determination of equilibrium Fe isotopic fractionation factors: application to goethite and jarosite. *Geochim. Cosmochim. Acta* **94**, 254−275.

Dauphas N., Janney P. E., Mendybaev R. A., Wadhwa M., Richter F. M., Davis A. M., Van Zuilen M., Hines R. and Foley C. N. (2004) Hromatographic separation and multicollection-ICPMS analysis of iron. Investigating mass-dependent and -independent isotope effects. *Anal. Chem.* **76**, 5855–5863.

Debret B. (2013) Serpentinites, vecteurs des circulations fluides et des transferts chimiques de l'océanisation à la subduction: exemple dans les Alpes occidentales. PhD thesis, Univ. Blaise Pascal, Clermont-Ferrand, France,

Debret B., Beunon H., Mattielli N., Andreani M., Ribeiro da Costa I. and Escartin J. (2018a) Ore component mobility, transport and mineralization at mid-oceanic ridges: A stable isotopes (Zn, Cu and Fe) study of the Rainbow massif (Mid-Atlantic Ridge 36°14′N). *Earth Planet. Sci. Lett.* **503**, 170–180.

Debret B., Bolfan-Casanova N., Padrón-Navarta J. A., Martin-Hernandez F., Andreani M., Garrido C. J., López Sánchez-Vizcaíno V., Gómez-Pugnaire M. T., Muñoz M. and Trcera N. (2015) Redox state of iron during high-pressure serpentinite dehydration. *Contrib. to Mineral. Petrol.* **169**.

Debret B, Bouilhol P., Pons M. L. and Williams H. (2018b) Carbonate Transfer during the Onset of Slab Devolatilization: New Insights from Fe and Zn Stable Isotopes. *J. Petrol.* **59**, 1145–1166.

Debret B., Millet M.-A., Pons M.-L., Bouilhol P., Inglis E. and Williams H. (2016) Isotopic evidence for iron mobility during subduction. *Geology* **44**, 215–218.

Debret B., Reekie C.D.J., Mattielli N., Beunon H., Ménez B., Savov I.P., Williams H. (2020) Redox transfer at subduction zones: insights from Fe isotopes in the Mariana forearc. *Geochemical Perspective Letters* **12**, 46-51.

Debret B. and Sverjensky D. A. (2017) Highly oxidising fluids generated during serpentinite breakdown in subduction zones. *Sci. Rep.* **7**.

Deschamps F., Godard M., Guillot S. and Hattori K. (2013) Geochemistry of subduction zone serpentinites: A review. *Lithos* **178**, 96–127. 10.1016/j.lithos.2013.05.019.

Dilissen N., Hidas K., Garrido C.J., Kahl W.A., López Sánchez-Vizcaíno V., Padrón-Navarta, J.A. (2018) Textural evolution during high-pressure dehydration of serpentinite to peridotite and its relation to stress orientations and kinematics of subducting slabs: Insights from the Almirez ultramafic massif. *Lithos* **320-321**, 470–489.

Ducher M., Blanchard M. and Balan E. (2016) Equilibrium zinc isotope fractionation in Zn-bearing minerals from first-principles calculations. *Chem. Geol.* **443**, 87–96.

Duncan M. S. and Dasgupta R. (2017) Rise of Earth's atmospheric oxygen controlled by efficient subduction of organic carbon. *Nat. Geosci.* **10**, 387–392.

Facq S., Daniel I., Montagnac G., Cardon H. and Sverjensky D. A. (2014) In situ Raman study and thermodynamic model of aqueous carbonate speciation in equilibrium with aragonite under subduction zone conditions. *Geochim. Cosmochim. Acta* **132**, 375–390.

Ferrando S., Petrelli M. and Frezzotti M. L. (2019) Gradual and selective trace-element enrichment in slab-released fluids at sub-arc depths. *Sci. Rep.* **9**, 1–9.

Fujii, T, Albarède, F. (2012) Ab initio calculation of the Zn isotope effect in phosphates, citrates, and malates and applications to plants and soil. *Plos One* **7**, doi:10.1371/journal.pone.0030726.

Fujii T., Moynier F., Blichert-Toft J. and Albarède F. (2014) Density functional theory estimation of isotope fractionation of Fe, Ni, Cu, and Zn among species relevant to geochemical and biological environments. *Geochim. Cosmochim. Acta* **140**, 553–576.

Garofalo P. S. (2012) The composition of Alpine marine sediments (Bündnerschiefer Formation, W Alps) and the mobility of their chemical components during orogenic metamorphism. *Lithos* **128**–**131**, 55–72. 10.1016/j.lithos.2011.10.009.

Garrido C. J., López Sánchez-Vizcaíno V., Gómez-Pugnaire M. T., Trommsdorff V., Alard O., Bodinier J. L. and Godard M. (2005) Enrichment of HFSE in chlorite-harzburgite produced by high-pressure dehydration of antigorite-serpentinite: Implications for subduction magmatism. *Geochemistry, Geophys. Geosystems* **6**.10.1029/2004gc000791.

Gerrits A. R., Inglis E. C., Dragovic B., Starr P. G., Baxter E. F. and Burton K. W. (2019) Release of oxidizing fluids in subduction zones recorded by iron isotope zonation in garnet. *Nat. Geosci.* **12**, 1029–1033.10.1038/s41561-019-0471-y.

Gómez-Pugnaire, M.T., Nieto, F., Abad, I., Velilla, N., Garrido, C.J., Acosta-Vigil, A., Barich, A., Hidas, K., López Sánchez-Vizcaíno, V. (2019). Alpine Metamorphism in the Betic Internal Zones, in: Quesada,

C., Oliveira, J.T. (Eds.), The Geology of Iberia: A Geodynamic Approach: Volume 3: The Alpine Cycle. Springer International Publishing, Cham, pp. 519-544.

Godard M., Lagabrielle Y., Alard O. and Harvey J. (2008) Geochemistry of the highly depleted peridotites drilled at ODP Sites 1272 and 1274 (Fifteen-Twenty Fracture Zone, Mid-Atlantic Ridge): Implications for mantle dynamics beneath a slow spreading ridge. *Earth Planet. Sci. Lett.* **267**, 410–425.

Groppo, C., Beltrando, M. and Compagnoni, R. (2008) The P–T path of the ultra-high pressure Lago di Cignana and adjoining high-pressure meta-ophiolitic units: insights into the evolution of the subducting Tethyan slab. *J. Metamorph. Geol.* **27**, 207–231.

Halama, R., Bebout, G., John, T. and Scambelluri M. (2014) Nitrogen recycling in subducted mantle rocks and implications for the global nitrogen cycle. *International Journal of Earth Sciences* **103**, 2081-2099.

Harvey J., Garrido C. J., Savov I., Agostini S., Padrón-Navarta J. A., Marchesi C., López Sánchez-Vizcaíno V. and Gómez-Pugnaire M. T. (2014) 11B-rich fluids in subduction zones: The role of antigorite dehydration in subducting slabs and boron isotope heterogeneity in the mantle. *Chem. Geol.* **376**, 20–30. 10.1016/j.chemgeo.2014.03.015.

Hermann J., Müntener O. and Scambelluri M. (2000) The importance of serpentinite mylonites for subduction and exhumation of oceanic crust. *Tectonophysics* **327**, 225-238.

Hill P. S. and Schauble E. A. (2008) Modeling the effects of bond environment on equilibrium iron isotope fractionation in ferric aquo-chloro complexes. *Geochim. Cosmochim. Acta* **72**, 1939–1958.

Huang J., Guo S., Jin Q.-Z. and Huang F. (2019) Iron and magnesium isotopic compositions of subduction-zone fluids and implications for arc volcanism. *Geochim. Cosmochim. Acta* **278**, 376-391.

Iacovino K., Guild M. R. and Till C. B. (2020) Aqueous fluids are effective oxidizing agents of the mantle in subduction zones. *Contrib. to Mineral. Petrol.* **175**, 36.

Inglis E. C., Debret B., Burton K. W., Millet M.-A., Pons M.-L., Dale C. W., Bouilhol P., Cooper M., Nowell G. M., McCoy-West A. J. and Williams H. M. (2017) The behavior of iron and zinc stable isotopes accompanying the subduction of mafic oceanic crust: A case study from Western Alpine ophiolites. *Geochemistry, Geophys. Geosystems* **18**.

Jabaloy-Sánchez, A., Gómez-Pugnaire, M.T., Padrón-Navarta, J.A., López Sánchez-Vizcaíno, V. and Garrido, C.J., (2015). Subduction- and exhumation-related structures preserved in metaserpentinites and associated metasediments from the Nevado–Filábride Complex (Betic Cordillera, SE Spain). *Tectonophysics* **644–645**, 40–57. 10.1016/j.tecto.2014.12.022.

John, T., Scambelluri, M., Frische, M., Barnes, J.D. and Bach, W. (2011). Dehydration of subducting serpentinite: implications for halogen mobility in subduction zones and the deep halogen. cycle. Earth Planet. Sci. Lett., **308**, 65– 76.

Johnson, C. M., Beard, B. L., Klein, C., Beukes, N. J. & Roden, E.E. (2008). Iron isotopes constrain biologic and abiologic processes in Banded Iron Formation genesis. *Geochimica et Cosmochimica Acta* **72**, 151–169.

Kelemen P. B. and Manning C. E. (2015) Reevaluating carbon fluxes in subduction zones, what goes down, mostly comes up. *Proc. Natl. Acad. Sci.* **112**, 3997–4006.

Kendrick, M.A., Scambelluri, M., Hermann, J., Padrón-Navarta, J.A. (2018). Halogens and noble gases in serpentinites and secondary peridotites: Implications for seawater subduction and the origin of mantle neon. *Geochimica et Cosmochimica Acta* **235**, 285–304. 10.1016/j.gca.2018.03.024.

El Korh A., Luais B., Deloule E. and Cividini D. (2017) Iron isotope fractionation in subduction-related high-pressure metabasites (Ile de Groix, France). *Contrib. to Mineral. Petrol.* **172**.

Laborda-López C., López-Sánchez-Vizcaíno V., Marchesi C., Gómez-Pugnaire M. T., Garrido C. J., Jabaloy-Sánchez A., Padrón-Navarta J. A. and Hidas K. (2018) High-P metamorphism of rodingites during

serpentinite dehydration (Cerro del Almirez, Southern Spain): Implications for the redox state in subduction zones. *J. Metamorph. Geol.* **36**, 1141–1173.

Li, X. P., Rahn, M. and Bucher, K. (2004). Serpentinites of the Zermatt-Saas ophiolite complex and their texture evolution. *J. Metamorph. Geol.* **22**, 159–177.

Liu S. and Li S. (2019) Tracing the Deep Carbon Cycle Using Metal Stable Isotopes : Opportunities and Challenges. *Engineering* **5**, 448–457.

Liu, S.A., Liu, P.P., Lv, Y., Wang, Z.Z. and Dai J.G. (2019). Cu and Zn isotope fractionation during oceanic alteration: Implications for Oceanic Cu and Zn cycles. *Geochim. Cosmochim. Acta* **257**, 191-205

Liu S. A., Wang Z. Z., Li S. G., Huang J. and Yang W. (2016) Zinc isotope evidence for a large-scale carbonated mantle beneath eastern China. *Earth Planet. Sci. Lett.* **444**, 169–178. http://dx.doi.org/10.1016/j.epsl.2016.03.051.

López Sánchez-Vizcaíno, V., Rubatto, D., Gómez-Pugnaire, M.T., Trommsdorff, V., Müntener, O. (2001). Middle Miocene high-pressure metamorphism and fast exhumation of the Nevado-Filabride Complex, SE Spain. *Terra Nova* **13**, 327–332.

López Sánchez-Vizcaíno V., Trommsdorff V., Gómez-Pugnaire M. T., Garrido C. J., Müntener O. and Connolly J. A. D. (2005) Petrology of titanian clinohumite and olivine at the high-pressure breakdown of antigorite serpentinite to chlorite harzburgite (Almirez Massif, S. Spain). *Contrib. to Mineral. Petrol.* **149**, 627–646.

Luoni P., Rebay G., Spalla M.I. and Zanoni D. (2018) UHP Ti-chondrodite in the Zermatt-Saas serpentinite: constraints on a new tectonic scenario. *Am. Mineral.* **103**, 1002-1005.

Maréchal, C.N., Télouk, P. and Albarède, F. (1999) Precise analysis of copper and zinc isotopic compositions by plasma-source mass spectrometry. *Chem. Geol.* **156**, 251–273.

Marchesi C., Garrido C. J., Padrón-Navarta J. A., López Sánchez-Vizcaíno V. and Gómez-Pugnaire M. T. (2013) Element mobility from seafloor serpentinization to high-pressure dehydration of antigorite in subducted serpentinite: Insights from the Cerro del Almirez ultramafic massif (southern Spain). *Lithos* **178**, 128–142.

Martin S., Rebay G., Kienast J.R. and Mevel C. (2008). An eclogitized oceanic palaeo-hydrothermal field from the St Marcel valley (Italian Western Alps). *Ofioliti* **33**, 49-63.

Martínez-Martínez, J.M., Soto, J.I., Balanyá, J.C. (2002). Orthogonal folding of extensional detachments: Structure and origin of the Sierra Nevada elongated dome (Betics, SE Spain). *Tectonics* **21**, 10.1029/2001tc001283.

Martínez-Martínez, J.M., Torres-Ruiz, J., Pesquera, A., Gil-Crespo, P.P. (2010). Geological relationships and U-Pb zircon and Ar^{40}/Ar^{39} tourmaline geochronology of gneisses and tourmalinites from the Nevado-Filabride complex (western Sierra Nevada, Spain): Tectonic implications. *Lithos* **119**, 238–250. 10.1016/j.lithos.2010.07.002.

Menzel M. D., Garrido C. J. and López Sánchez-Vizcaíno V. (2020) Fluid-mediated carbon release from serpentinite-hosted carbonates during dehydration of antigorite-serpentinite in subduction zones. **531**, 115964.

Menzel, M.D., Garrido, C.J., López Sánchez-Vizcaíno, V., Hidas, K., Marchesi, C. (2019). Subduction metamorphism of serpentinite-hosted carbonates beyond antigorite-serpentinite dehydration (Nevado-Filábride Complex, Spain). *Journal of Metamorphic Geology* **37**, 681–715. 10.1111/jmg.12481.

Milesi V., Guyot F., Brunet F., Richard L., Recham N., Benedetti M., Dairou J. and Prinzhofer A. (2015) Formation of CO2, H2 and condensed carbon from siderite dissolution in the 200-300°C range and at 50MPa. *Geochim. Cosmochim. Acta*. **154**, 201-211.

Moeller K., Schoenberg R., Pedersen R. B., Weiss D. and Dong S. (2012) Calibration of the New Certified Reference Materials ERM-AE633 and ERM-AE647 for Copper and IRMM-3702 for Zinc Isotope Amount Ratio Determinations. *Geostand. Geoanalytical Res.* **36**, 177–199.

Moynier F., Albarède F. and Herzog G. F. (2006) Isotopic composition of zinc, copper, and iron in lunar samples. *Geochim. Cosmochim. Acta* **70**, 6103–6117.

Moynier F., Vance D., Fujii T. and Savage P. (2017) The isotope geochemistry of zinc and copper. *Non-Traditional Stable Isot.* **82**, 543–600.

Nimis P. and Trommsdorff V. (2001) Revised thermobarometry of Alpe Arami and other garnet peridotites from the Central Alps. *J. Petrol.* **42**, 103-115.

Niu Y. (2004) Bulk-rock major and trace element compositions of abyssal peridotites: Implications for mantle melting, melt extraction and post-melting processes beneath Mid-Ocean ridges. *J. Petrol.* **45**, 2423–2458.

Padrón-Navarta J.-A., Hermann J., Garrido C. J., Lopez Sánchez-Vizcaíno V. and Gómez-Pugnaire M. T. (2010b) An experimental investigation of antigorite dehydration in natural silica-enriched serpentinite. , 25–42.

Padrón-Navarta J. A., López Sánchez-Vizcaíno V., Garrido C. J. and Gómez-Pugnaire M. T. (2011) Metamorphic record of high-pressure dehydration of antigorite serpentinite to chlorite harzburgite in a subduction setting (Cerro del Almirez, Nevado-Filábride complex, Southern Spain). *J. Petrol.* **52**, 2047–2078.

Padrón-Navarta J. A., López Sánchez-Vizcaíno V., Garrido C. J., Gómez-Pugnaire M. T., Jabaloy A., Capitani G. C. and Mellini M. (2008) Highly ordered antigorite from Cerro del Almirez HP-HT serpentinites, SE Spain. *Contrib. to Mineral. Petrol.* **156**, 679–688.

Padrón-Navarta, J.A., Tommasi, A., Garrido, C.J., Mainprice, D. (2015) On topotaxy and compaction during antigorite and chlorite dehydration: an experimental and natural study. *Contributions to Mineralogy and Petrology* **169**, 1–20. 10.1007/s00410-015-1129-4.

Padrón-Navarta J. A., Tommasi A., Garrido C. J., López Sánchez-Vizcaíno V., Gómez-Pugnaire M. T., Jabaloy A. and Vauchez A. (2010a) Fluid transfer into the wedge controlled by high-pressure hydrofracturing in the cold top-slab mantle. *Earth Planet. Sci. Lett.* **297**, 271–286.

Pan D., Spanu L., Harrison B., Sverjensky D. A. and Galli G. (2013) Dielectric properties of water under extreme conditions and transport of carbonates in the deep Earth. *Proc. Natl. Acad. Sci.* **110**.

Paulick H., Bach W., Godard M., de Hoog C.-J., Suhr G. and Harvey J. (2006) ODP Leg 209: Implications for fluid / rock interaction in slow spreading environments. *Chem. Geol.* **234**, 179–210.

Pelletier, L. and Müntener O. (2006) High-pressure metamorphism of the Lanzo peridotite and its oceanic cover, and some consequences for the Sezia-Lanzo zone (northwestern Italian Alps). *Lithos* **90**, 111–130.

Plank T. and Manning C. E. (2019) Subducting carbon. *Nature* **574**, 343–352.

Poitrasson F., Delpech G. and Gregoire M. (2013) On the iron isotope heterogeneity of lithospheric mantle xenoliths : implications for mantle metasomatism, the origin of basalts and the iron isotope composition of the Earth. *Contrib. to Mineral. Petrol.* **165**, 1243–1258.

Polyakov V. B. and Mineev S. D. (2000) The use of Mossbauer spectroscopy in stable isotope geochemistry. *Geochim. Cosmochim. Acta* **64**, 849–865.

Pons M.-L., Debret B., Bouilhol P., Delacour A. and Williams H. (2016) Zinc isotope evidence for sulfate-rich fluid transfer across subduction zones. *Nat. Commun.* **7**, 13794.

Puga, E., Fanning, M., Díaz De Federico, A., Nieto, J.M., Beccaluva, L., Bianchini, G., Díaz Puga, M.A. (2011). Petrology, geochemistry and U-Pb geochronology of the Betic Ophiolites: Inferences for Pangaea break-up and birth of the westernmost Tethys Ocean. *Lithos* **124**, 255–272. 10.1016/j.lithos.2011.01.002.

Ravna, E.J.K., Andersen, B., Jolivet, L. and De Capitani, C. (2010) Cold subduction and the formation of lawsonite eclogite – constraints from prograde evolution of eclogitized pillow lava from Corsica. *J. Metamorph. Geol.* **28**, 381–395.

Reinecke, T. (1998) Prograde high-to ultrahigh-pressure metamorphism and exhumation of oceanic sediments at Lago di Cignana, Zermatt-Saas Zone, western Alps. *Lithos* **42**, 147–189.

Scambelluri M., Cannao E. and Gilio M. (2019) The water and fluid-mobile element cycles during serpentinite subduction. A review. *Eur. J. Mineral.*, 1–24.

Scambelluri, M., Bebout, B. E., Belmonte, D., Gilio, M., Campomenosi, N., Collins, N. and Crispini, L. (2016). Carbonation of subduction-zone serpentinite (high-pressure ophicarbonate; Ligurian Western Alps) and implications for the deep carbon cycling. *Earth Planet. Sci. Lett.* **441**, 155–166.

Scambelluri M., Fiebig J., Malaspina N., Müntener O. and Pettke T. (2004a) Serpentinite Subduction : Implications for Fluid Processes and Trace-Element Recycling. *Int. Geol. Rev.* **46**, 595–613.

Scambelluri M., Müntener O., Ottolini L., Pettke T. and Vannucci R. (2004b) The fate of B , Cl and Li in the subducted oceanic mantle and in the antigorite breakdown fluids. *Earth Planet. Sci. Lett.* **222**, 217–234.

Scambelluri M., Pettke T. and Cannaò E. (2015) Fluid-related inclusions in Alpine high-pressure peridotite reveal trace element recycling during subduction-zone dehydration of serpentinized mantle (Cima di Gagnone, Swiss Alps). *Earth Planet. Sci. Lett.* **429**, 45–59.

Schauble E. A. (2004) Fractionation theory to new systems. *Rev. Mineral. Geochemistry* **55**, 65–111.

Schwartz, S., Guillot, S., Reynard, B., Lafay, R., Debret, B., Nicollet, C., Lanari, P. and Auzende, A.L. (2013) Pressure-temperature estimates of the lizardite/antigorite transition in high pressure serpentinites. *Lithos* **178**, 197–210.

Shen J., Li S., Wang S., Teng F. and Li Q. (2018) Subducted Mg-rich carbonates into the deep mantle wedge. *Earth Planet. Sci. Lett.* **503**, 118–130.

Snow, J.E., Dick, H.J.B. (1995) Pervasive magnesium loss by marine weathering of peridotite. *Geochim. Cosmochim. Acta* **59**, 4219–4235.

Sossi P. A., Nebel O. and Foden J. (2016) Iron isotope systematics in planetary reservoirs. *Earth Planet. Sci. Lett.* **1**, 1–14. Available at: http://dx.doi.org/10.1016/j.epsl.2016.07.032.

Sossi P. A., Nebel O., O'Neill H. S. C. and Moynier F. (2018) Zinc isotope composition of the Earth and its behaviour during planetary accretion. *Chem. Geol.* **477**, 73–84. 10.1016/j.chemgeo.2017.12.006.

Sverjensky D. A., Stagno V. and Huang F. (2014) Important role for organic carbon in subduction-zone fluids in the deep carbon cycle. *Nat. Geosci.* **7**, 909–913.

Syracuse E. M., van Keken P. E. and Abers G. A. (2010). The global range of subduction zone thermal models. *Physics of the Earth and Planetary Interiors* 183, 73-90.

Trommsdorff V., López Sánchez-Vizcaíno V., Gómez-Pugnaire M. T. and Müntener O. (1998) High pressure breakdown of antigorite to spinifex-textured olivine and orthopyroxene, SE Spain. *Contrib. to Mineral. Petrol.* **132**, 139–148.

Turner S., Williams H., Piazolo S., Blichert-Toft J., Gerdes M., Adam J., Liu X. M., Schaefer B. and Maury R. (2018) Sub-arc xenolith Fe-Li-Pb isotopes and textures tell tales of their journey through the mantle wedge and crust. *Geology* **46**, 947–950.

Ulmer, P. and Trommsdorff, V. (1995). Serpentine Stability to Mantle Depths and Subduction-Related Magmatism. Science **268**, 858–861. https://doi.org/10.1126/science.268.5212.858

Vitale Brovarone, A., Groppo, C., Hetenyi, G., Compagnoni, R. and Malavieille, J. (2011) Coexistence of lawsonite-eclogite and blueschist: phase diagram calculations from Alpine Corsica metabasalts. *J. Metamorph. Geol.* **29**, 583-600.

Wang Z.Z., Liu S.-A., Liu J., Huang J., Xiao Y., Chu Z.Y., Zhao X.-M. and Tang L. (2017) Zinc isotope fractionation during mantle melting and constraints on the Zn isotope composition of Earth's upper mantle. *Geochim. Cosmochim. Acta* **198**, 151–167.

Weyer S. and Ionov D. A. (2007) Partial melting and melt percolation in the mantle: The message from Fe isotopes. *Earth Planet. Sci. Lett.* **259**, 119–133.

Williams H. M. and Bizimis M. (2014) Iron isotope tracing of mantle heterogeneity within the source regions of oceanic basalts. *Earth Planet. Sci. Lett.* **404**, 396–407.

Williams H.M., Peslier A.H., McCammon C., Halliday A.N., Levasseur S., Teutsch N. and Burg J.P. (2005) Systematic iron isotope variations in mantle rocks and minerals: The effects of partial melting and oxygen fugacity. *Earth Planet. Sci. Lett.* **235**, 435−452.

Wunder B. and Schreyer W. (1997) Antigorite : High-pressure stability in the system MgO-SiO2-H2O (MSH). *Lithos* **41**, 213–227.

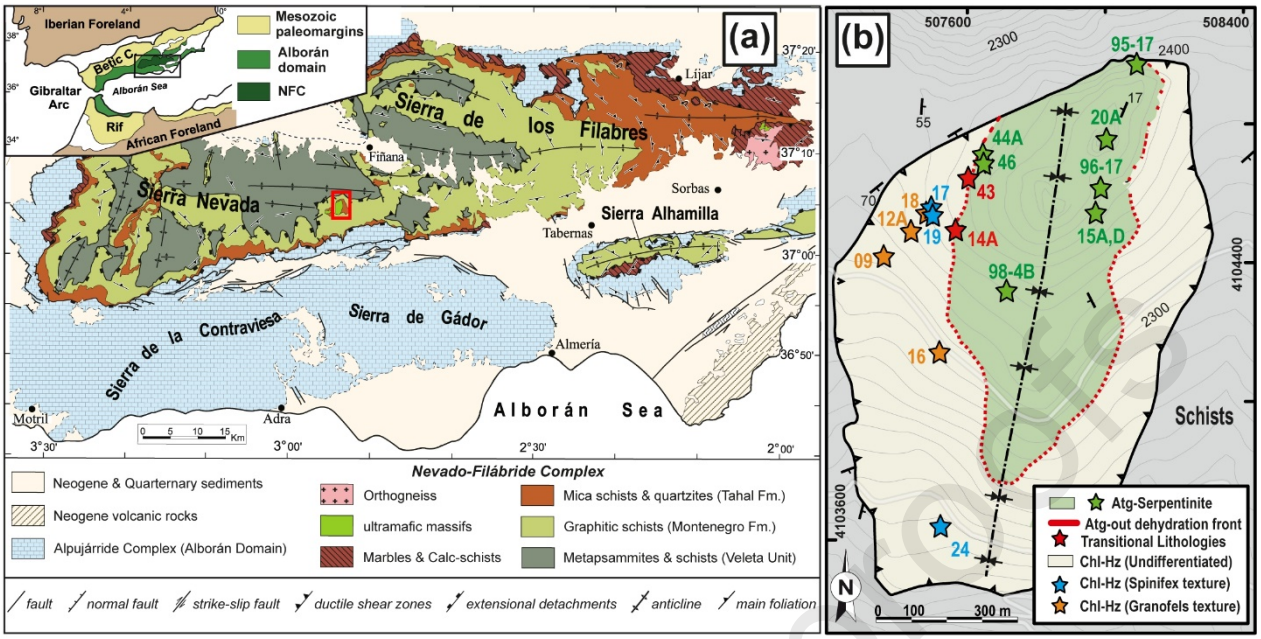

Figure 1: (a) Geological map of the Nevado-Filábride Complex (NFC) in the central part of the Betic Cordillera (South Spain), showing the location of the ultramafic massifs and the Cerro del Almirez (red rectangle); modified from Martinez-Martinez et al. (2010) and Menzel et al. (2019). Inset. Location of the study area in the Betic-Rif belt. (b) Geological map of the Cerro del Almirez ultramafic showing the main lithologies; modified from Jabaloy et al. (2015) and Dilissen et al. (2018). Stars indicate the position of representative samples selected for the present study (see Table 1 for more details on sample lithology).

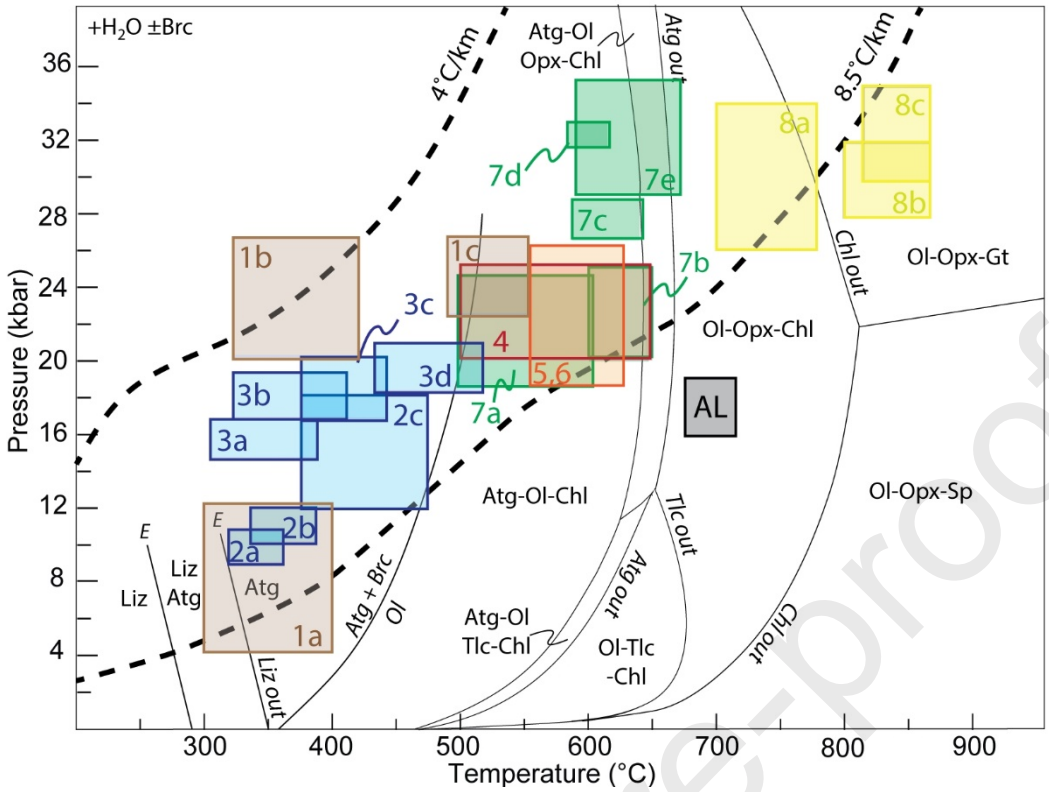

Figure 2: Compilation of P-T data for alpine meta-ophiolites. Cold (4°C/km) and hot (8.5 °C/km) slab geotherms are from Syracuse et al. (2010). The metamorphic reaction pseudosection is from Debret et al. (2015). All of alpine meta-ophiolites are coherent with slab geotherms between 4°C/km and 8.5°C/km with exception of the Cerro del Almirez massif which shows abnormally high temperature conditions. Alpine Corsica including Monte Maggiore (1a: Debret, 2013), Défilé de Lancone (1b: Ravna et al., 2010), San Petrone (1c: Vitale-Brovarone et al., 2011); 2-7: Western Alps including Queyras ophiolite complex (2: Schwartz et al., 2013; 3: Agard et al., 2001); Erro Tobbio (4: Hermann et al., 2000); Monviso (5: Schwartz et al., 2001 ; Angiboust et al., 2011); Lanzo (6: Pelletier and Muntener, 2006); Zermatt Saas ophiolite complex (7a: Martin et al., 2008; 7b:Li et al., 2004; 7c: Reinecke et al., 1998; 7d: Groppo et al., 2008; 7e: Luoni et al., 2018); Central Alps including Cima di Gagnone (8a), Monte Duria (8b) and Alpe Arami (8c; Nimis and Trommsdorff, 2001); AL: Cerro del Almirez (López Sánchez-Vizcaíno et al., 2005; Laborda-López et al., 2018).

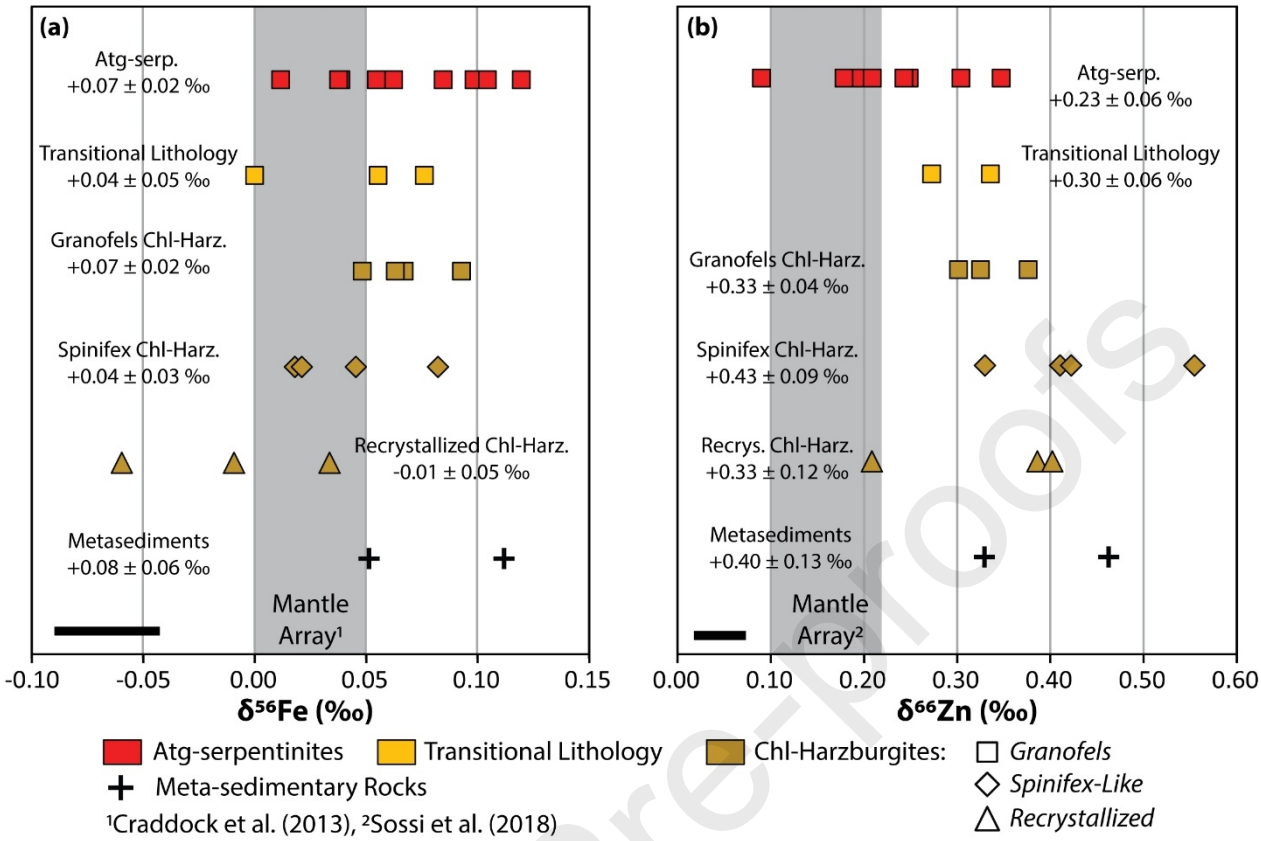

Figure 3: Fe and Zn isotopic ranges of each major lithological division of the Cerro del Almirez massif. The black bar correspond to long term reproducibility on FeCl (± 0.05 ‰) and Alpha Asear (± 0.035 ‰) for Fe and Zn stable isotopes, respectively. The average value of each lithology is given on the figure.

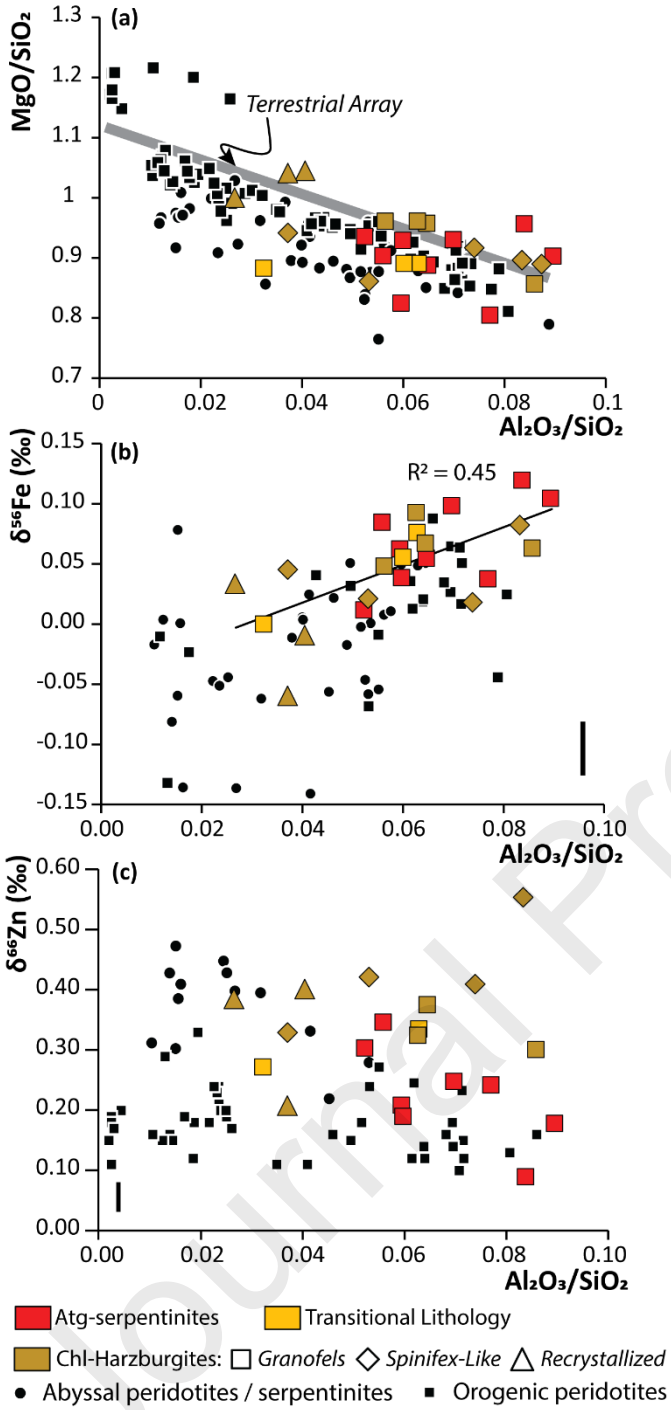

Figure 4: Plots of Al_2O_3/SiO_2 versus (a) MgO/SiO_2, (b) $\delta^{56}Fe$ and (c) $\delta^{66}Zn$ in Cerro del Almirez ultramafic rocks. The thick grey line on Fig. 4a represent the bulk silicate earth ("terrestrial array" after Jagoutz et al., 1979). Abyssal peridotites and serpentinites values are from Craddock et al. (2013), Debret et al. (2018a)

and Liu et al. (2019). Orogenic peridotites values are from Weyer and Ionov (2007), Debret et al. (2016), Pons et al. (2016), Wang et al. (2017), Sossi et al. (2018) and Liu et al.(2019).

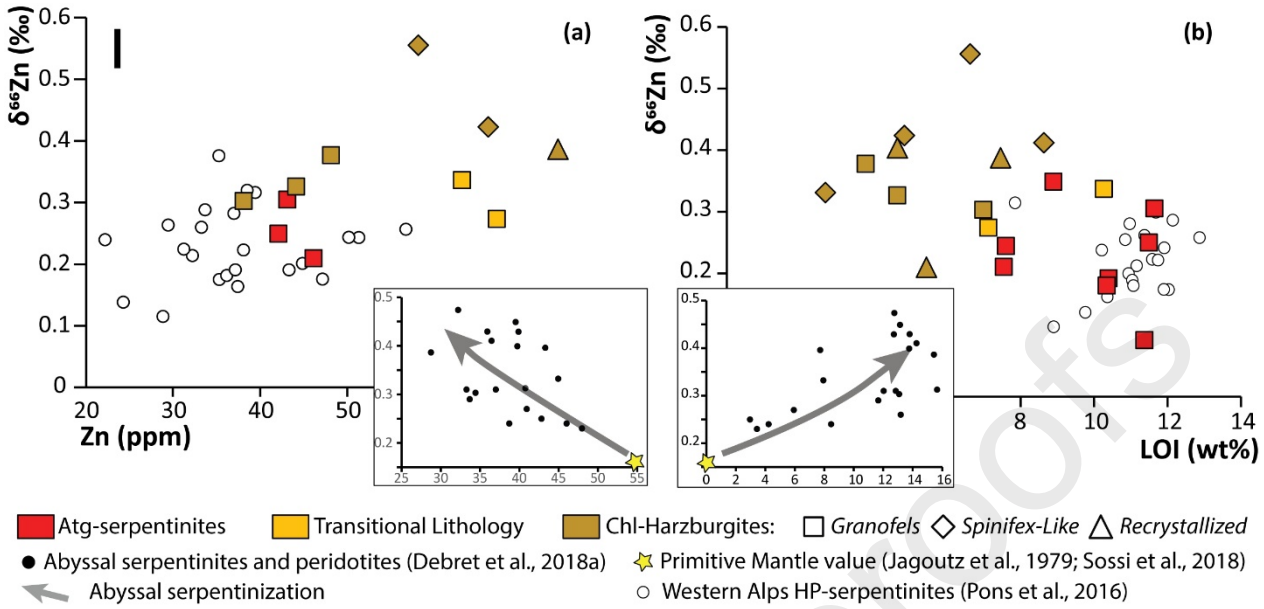

Figure 5: Plots of $\delta^{66}Zn$ versus (a) Zn concentrations and (b) Loss On Ignition (LOI) in Cerro del Almirez ultramafic rocks. The isotopic composition of metamorphic serpentinites from Western Alps meta-ophiolites is shown for comparison and is similar to that of Atg-serpentinites. The small panels show published Zn isotope, Zn concentration and LOI data for abyssal peridotites and serpentinites (after Debret et al., 2018a). Note that broad arrays defined by the Cerro del Almirez ultramafic rocks are opposite in nature to those observed in abyssal settings.

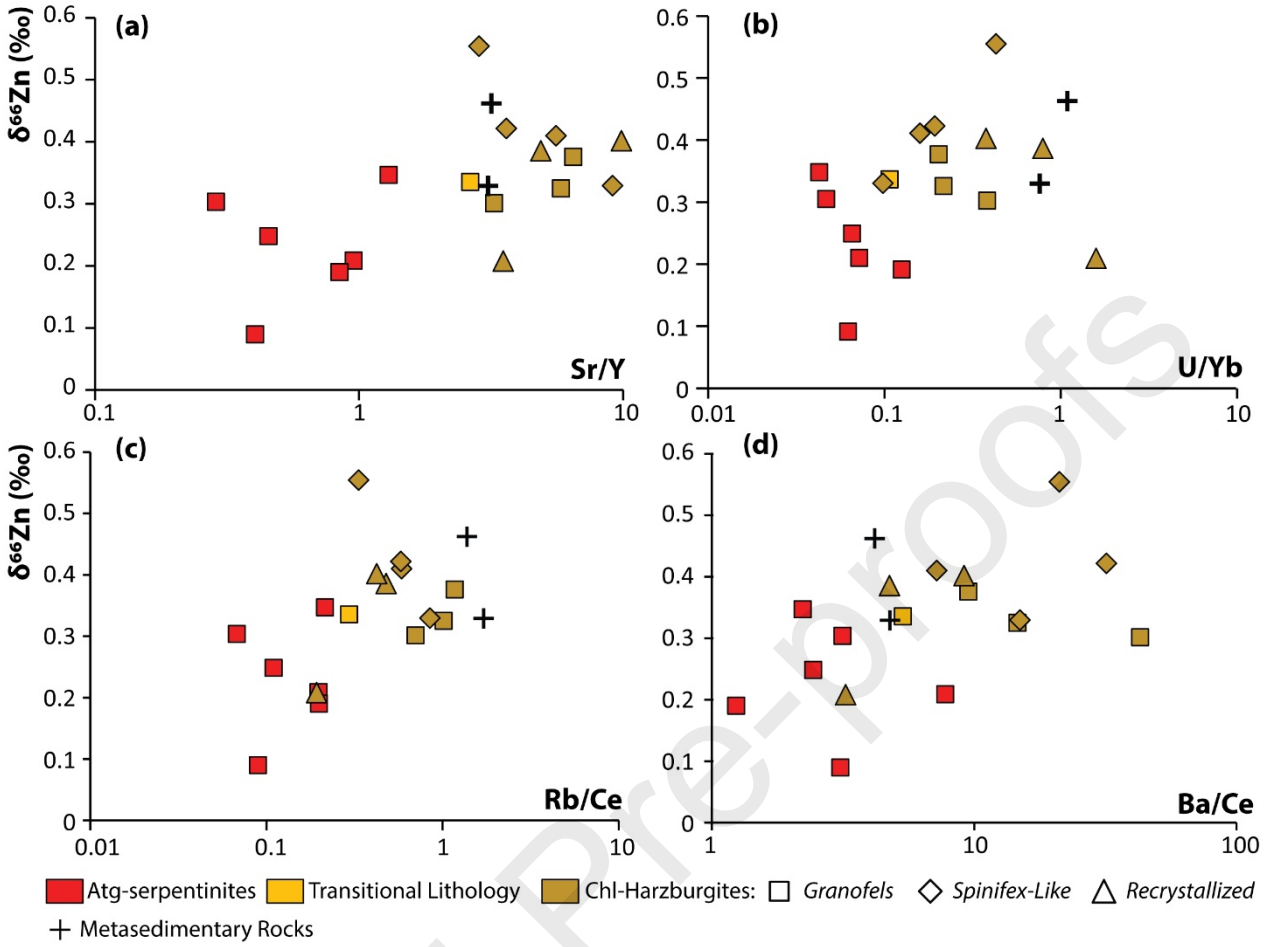

Figure 6: Plots of $\delta^{66}Zn$ versus (a) Sr/Y, (b) U/Yb, (c) Rb/Ce and (d) Ba/Ce ratios in Cerro del Almirez meta-serpentinites.

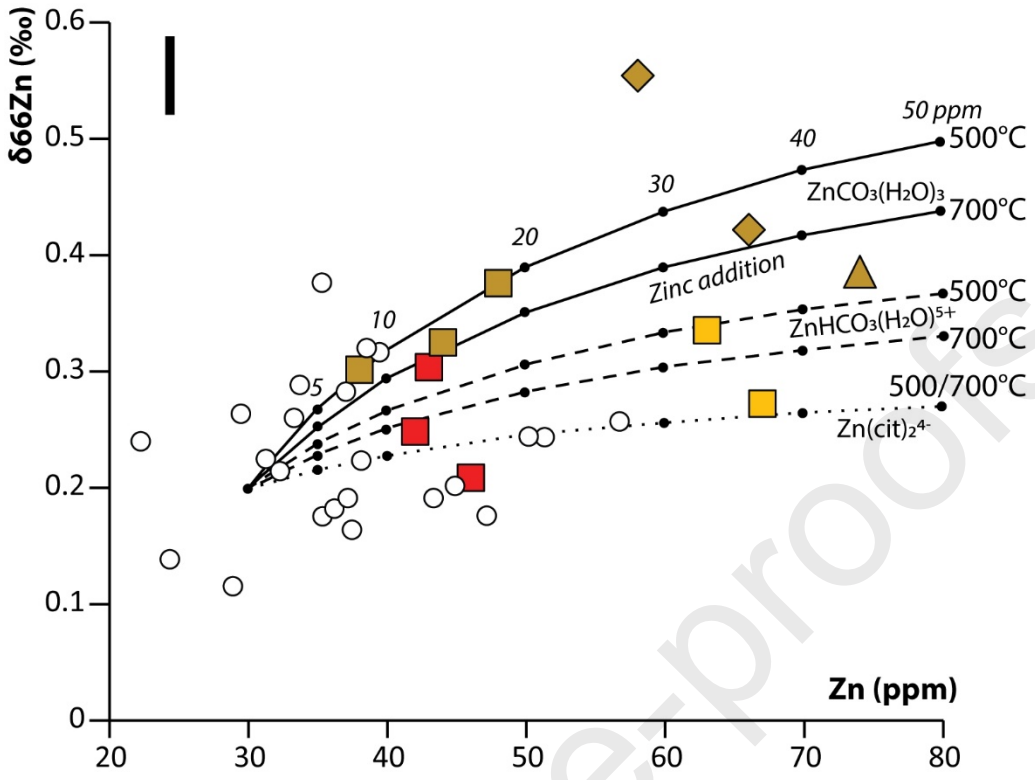

Figure 7: Plot of $\delta^{66}Zn$ (‰) versus Zn concentrations in Cerro del Almirez samples and presenting the results of the mixing models: additions of Zn by $ZnCO_3(H_2O)_3$, $ZnHCO_3(H_2O)_5^+$ and $Zn(cit)_2^{4-}$ fluids at temperatures ranging from 500°C to 700°C.

Name	Rock Type	Minerals	FeO (wt%)	Zn (ppm)	δ^{56}Fe (‰)	2sd	δ^{57}Fe (‰)	2sd	n	δ^{66}Zn (‰)	2sd	n
AL06-44A	Atg-serpentinite	Atg-Ol-Chl-Mgt ±Ilm	6.71	42	0.10	0.06	0.14	0.03	5	0.25	0.03	3
AL06-46	Atg-serpentinite	Atg-Ol-Chl-Mgt ±Ilm	7.04	43	0.01	0.01	0.02	0.04	3	0.30	0.04	3
ALM98-04B	Atg-serpentinite	Atg-Ol-Chl-Mgt ±Ilm	7.51	-	0.12	0.04	0.19	0.09	3	0.09	0.02	5
AL06-09A	Atg-serpentinite	Atg-Ol-Chl-Mgt ±Ilm-Di-Tr	9.87	46	0.06	0.03	0.12	0.10	2	0.21	0.05	5
AL95-17	Atg-serpentinite	Atg-Ol-Chl-Mgt ±Ilm-Di	6.68	-	0.04	-	0.07	-	1	0.19	0.05	2
AL96-17	Atg-serpentinite	Atg-Ol-Chl-Mgt ±Ilm-Di-Tr	7.66	-	0.08	-	0.10	-	1	0.35	0.02	3
AL06-20A	Atg-serpentinite	Atg-Ol-Chl-Mgt ±Ilm	7.33	34	0.05	0.02	0.09	0.07	4	-	-	
AL96-15A	Atg-serpentinite	Atg-Ol-Chl-Mgt ±Ilm-TiChu	8.96	-	0.10	0.03	0.16	0.08	3	0.18	0.00	2
AL96-15D	Atg-serpentinite	Atg-Ol-Chl-Mgt ±Ilm-TiChu	8.97	-	0.04	0.04	0.07	0.05	4	0.24	0.03	3
AL06-43	Transitional Lithologies	Atg-Ol-Chl-Mgt ±Ilm-Opx	7.17	63	0.08	0.01	0.09	0.04	5	0.34	0.03	3
AL07-06	Transitional Lithologies	Atg-Ol-Chl-Mgt ±Ilm-Opx	7.77	45	0.06	0.04	0.07	0.05	2	-	-	
AL08-14A	Transitional Lithologies	Atg-Ol-Chl-Mgt ±Ilm-Opx	8.70	67	0.00	0.03	0.01	0.11	2	0.27	0.01	3
AL06-12A	Granofels Chl-harzburgites	Ol-Opx-Chl-Mgt ±Ilm/Hem	7.73	48	0.07	0.04	0.11	0.07	4	0.38	0.01	2
AL07-09	Granofels Chl-harzburgites	Ol-Opx-Chl-Mgt ±Ilm/Hem	7.86	44	0.09	0.07	0.14	0.03	4	0.33	0.02	3
AL08-16	Granofels Chl-harzburgites	Ol-Opx-Chl-Mgt ±Ilm/Hem	8.11	59	0.06	0.03	0.08	0.03	3	-	-	
AL06-18	Granofels Chl-harzburgites	Ol-Opx-Chl-Mgt ±Ilm/Hem	6.89	38	0.02	0.06	0.03	0.14	4	0.30	0.04	6
AL95-29	Spinifex Chl-harzburgites	Ol-Opx-Chl-Mgt ±Ilm/Hem	8.08	-	0.05	0.04	0.07	0.07	5	0.33	0.05	3
AL06-17	Spinifex Chl-harzburgites	Ol-Opx-Chl-Mgt ±Ilm/Hem	7.53	58	0.08	0.02	0.10	0.04	4	0.55	0.09	2
AL95-24	Spinifex Chl-harzburgites	Ol-Opx-Chl-Mgt ±Ilm/Hem	6.98	-	0.02	0.03	0.05	0.02	3	0.40	0.04	3
AL06-19	Spinifex Chl-harzburgites	Ol-Opx-Chl-Mgt ±Ilm/Hem	7.32	66	0.02	0.06	0.05	0.15	2	0.42	0.02	5
AL06-03A	Recrystallized Chl-harzburgites	Ol-Opx-Chl-Mgt ±Ilm/Hem	7.67	74	0.03	0.02	0.07	0.02	7	0.41	0.06	6

AL95-26	Recrystallized Chl-harzburgites	Ol-Opx-Chl-Mgt ±Ilm/Hem	7.46	-	-0.01	0.05	-0.05	0.07	5	0.49	0.03 3
AL96-1A	Recrystallized Chl-harzburgites	Ol-Opx-Chl-Mgt ±Ilm/Hem	7.28	-	-0.06	0.07	-0.12	0.13	2	0.21	0.04 3
AL96-12A	Metasedimentary rock	Graphite-lacking Micaschist	8.26	125	0.05	0.04	0.07	0.05	2	0.46	0.03 6
AL98-14A	Metasedimentary rock	Graphite-rich Micaschist	6.44	113	0.11	0.03	0.17	0.04	2	0.33	0.04 6
BHVO-2	Basalt standard	-			-	-	-	-		0.35	0.05 2
BIR	Basalt standard	-			0.06	0.02	0.08	0.01	2	-	-

Table 1: Fe and Zn isotope ratios of Cerro del Almirez ultramafic and metasedimentary rocks and standards. Atg: antigorite, Ol: olivine, Opx: orthopyroxene, Chl: chlorite, Mgt: magnetite, Ilm: ilmenite, Hem: hematite